Marine Pollution Bulletin 173 (2021) 112930

Contents lists available at ScienceDirect

Marine Pollution Bulletin

journal homepage: www.elsevier.com/locate/marpolbul

Insights from barium variability in a *Siderastrea siderea* coral in the northwestern Gulf of Mexico

Mudith M. Weerabaddana [a,b], Kristine L. DeLong [a,c,*], Amy J. Wagner [d], Deborah W.Y. Loke [a], K. Halimeda Kilbourne [e], Niall Slowey [f], Hsun-Ming Hu [g], Chuan-Chou Shen [g]

[a] Department of Geography and Anthropology, Louisiana State University, 227 Howe-Russell Geoscience Complex, Baton Rouge, LA 70803, USA
[b] Plentzia Marine Station, University of the Basque Country, 48620 Plentzia, Bizkaia, Basque Country, Spain
[c] Coastal Studies Institute, Louisiana State University, 331 Howe-Russell Geoscience Complex, Baton Rouge, LA 70803, USA
[d] Department of Geology, California State University, 6000 J. Street, Sacramento, CA 95819, USA
[e] Chesapeake Bay Marine Laboratory, University of Maryland, P.O. Box 775, Cambridge, MD 21613, USA
[f] Texas A&M University, College Station, TX 77843-3146, USA
[g] High-precision Mass Spectrometry and Environment Change Laboratory (HISPEC) and Research Center for Future Earth, Department of Geosciences, National Taiwan University, No. 1, Sec. 4, Roosevelt Rd., Taipei 10617, Taiwan, ROC

ARTICLE INFO

Keywords:
Coral Ba/Ca
Coral Sr/Ca
Barite
Drilling mud
Productivity
Flower Garden Banks

ABSTRACT

Coral Ba/Ca is a proxy for seawater barium concentration that varies with upwelling, terrigenous input, and marine productivity whereas coral Sr/Ca varies with temperature. We examine monthly coral Ba/Ca and Sr/Ca before and during offshore oil exploration in a *Siderastrea siderea* coral from West Flower Garden Bank located on the continental shelf edge in the Gulf of Mexico. Coral Ba/Ca variations lack pulses driven by upwelling or river outflow and are not in sync with coral Sr/Ca that exhibit a different seasonal pattern. Seasonal variations in chlorophyll-a concentration negatively correlate with coral Ba/Ca explaining 25% of that variability. A significant increase in mean coral Ba/Ca of 1.76 μmol/mol between 1931–1944 and 1976–2004 corresponds to the increase in the United States barite production and consumption primarily used in offshore oil drilling, which escalated in the 1970s, suggesting oil drilling operations are increasing seawater Ba concentration in the Gulf of Mexico.

1. Introduction

The Gulf of Mexico is the most explored, drilled, and developed offshore oil province in the world (Priest, 2007) (Fig. 1a). Oil discovery in coastal Louisiana in 1938 led to the first oil platform in the northern Gulf of Mexico in 1947 followed by an offshore oil production boom into the 1970s (Priest, 2007). Oil exploration moved from coastal waters to deeper ocean sites and by the end of the twentieth century with more than 70% of the Gulf of Mexico's oil production coming from wells (more than 40,000) in water depths greater than 300 m (Turner et al., 2004).

Flower Garden Banks National Marine Sanctuary in the northern Gulf of Mexico is a unique location for coral reefs because they are located in the open ocean on rising submerged salt domes at the edge of the wide continental shelf, ~185 km to the closest landmass (Fig. 1a). The sanctuary has two coral reefs (East and West) (Fig. 1b) and these reefs are in deeper water (18–40 m) than other coral reefs in the southern Gulf of Mexico, are located far from river runoff and coastal upwelling, and thus these two coral reefs are some of the healthiest in the United States (US) waters with 50% live coral coverage (Schmahl et al., 2008). Additionally, there are several oil platforms in close vicinity to Flower Garden Banks accessing the petroleum deposits under the salt domes. The unique geographic location of the Flower Garden Banks is ideal for evaluating the impact of oil drilling operations and marine environmental forcing on corals in this economically important part of the Gulf of Mexico.

Massive long-lived scleractinian corals are environmental archives that contain geochemical proxies (e.g., Sr/Ca, Ba/Ca, Mg/Ca) of past environmental and climatic changes (Corrège, 2006; Guzmán and Tudhope, 1998; Lough and Cooper, 2011; Sadler et al., 2014). Corals construct an aragonite exoskeleton, a mineral form of calcium carbonate

* Corresponding authors.
E-mail addresses: mudithw@email.arizona.edu (M.M. Weerabaddana), kdelong@lsu.edu (K.L. DeLong), amy.wagner@csus.edu (A.J. Wagner), kilbourn@umces.edu (K.H. Kilbourne), slowey@tamu.edu (N. Slowey), river@ntu.edu.tw (C.-C. Shen).

https://doi.org/10.1016/j.marpolbul.2021.112930
Received 9 April 2021; Received in revised form 31 August 2021; Accepted 1 September 2021

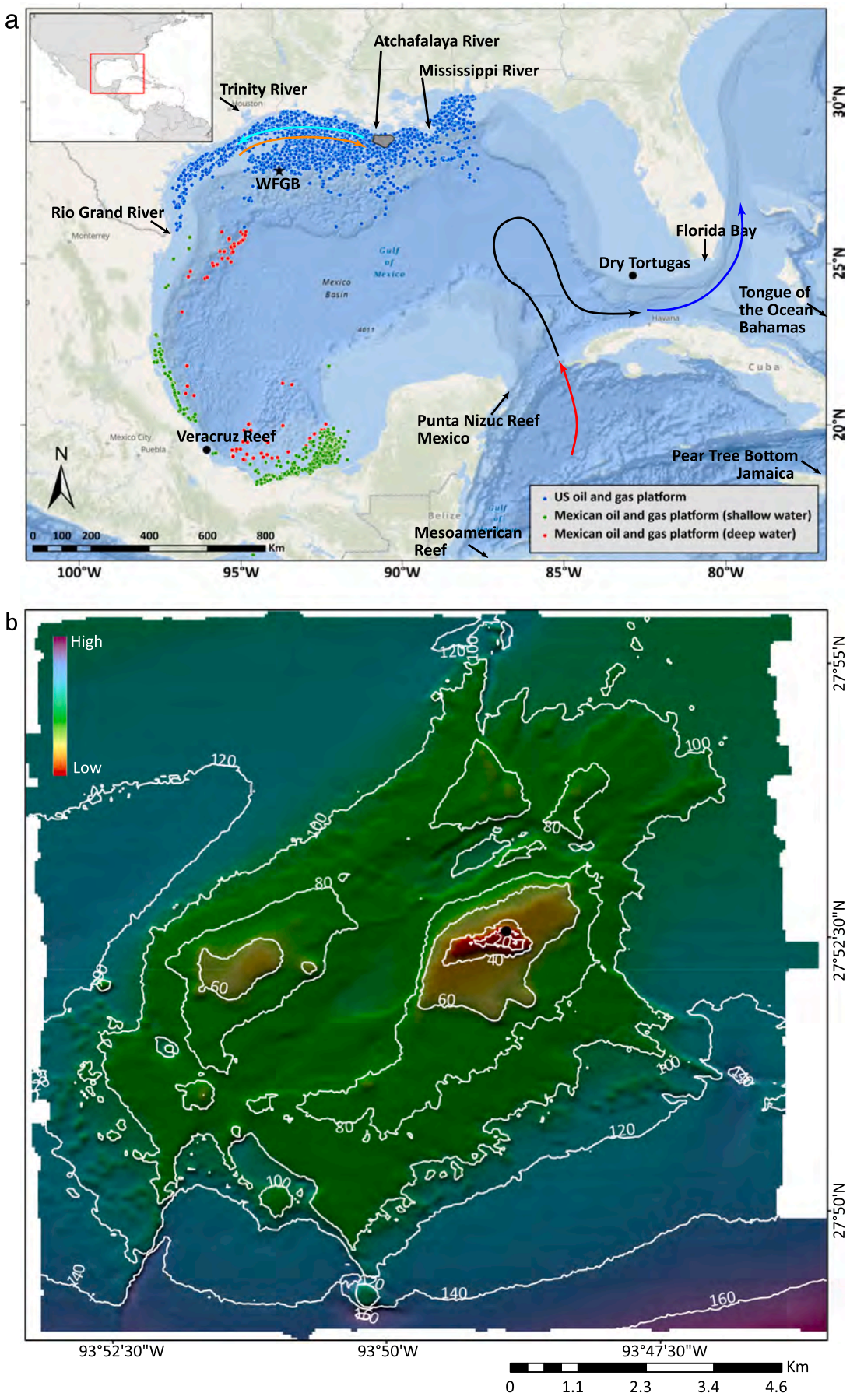

(caption on next page)

Fig. 1. The locations of West Flower Garden Bank (WFGB) and the oil and gas platforms in the Gulf of Mexico (a). Shapefiles for the United States and Mexican oil platforms are from the Bureau of Ocean Energy Management (www.boem.gov) and the Centro Nacional de Información de Hidrocarburos (mapa.hidrocarburos.gob.mx), respectively. The approximate locations of predominant currents are shown including the Caribbean Current entering the Gulf (red line), the Loop Current (black line) that leaves the Gulf of Mexico through the Straits of Florida becoming the Florida Current (blue line). Northern Gulf of Mexico coastal currents that transport Mississippi and Atchafalaya rivers' discharge (Walker, 2005) are shown for winter (cyan arrow) and summer (orange arrow). The grey area is the approximate area of the hypoxia zone (>75% chance of occurrence) that develops west of the mouth of the Mississippi River (Rabalais et al., 2002). Bathymetry of WFGB from https://pubs.usgs.gov/of/2002/0411/data.html (b). The *S. siderea* colony sampled in this study is located on the north side of WFGB at a water depth of 23.8 m (black dot). Other nearby Atlantic coral locations are noted (Table 1). (For interpretation of the references to colour in this figure legend, the reader is referred to the web version of this article.)

($CaCO_3$), and exhibit annual density bands where a couplet of high and low-density bands represent approximately one year of growth (Buddemeier and Maragos, 1974; Knutson et al., 1972). Annual density bands allow for the time assignment of the geochemical variations in the coral skeleton obtained from samples extracted along the growth trajectory in the coral that can be sampled with subannual resolution. Corals incorporate barium (Ba) in their skeleton as a function of seawater concentration (LaVigne et al., 2016; Lea et al., 1989; Livingston and Thompson, 1971; Montaggioni et al., 2006). Strontium (Sr) and magnesium (Mg) tend to vary in the coral skeleton as a function of temperature because their seawater concentrations are generally conservative on 1000-year time scales (Mitsuguchi et al., 1996; Smith et al., 1979; Weber, 1973; Weber, 1974). The calibration equations for coral Sr/Ca to temperature vary with geographical location, species, and water depth (Alibert and McCulloch, 1997; Corrège, 2006; DeLong et al., 2011; Goodkin et al., 2007; Sadler et al., 2014; Swart et al., 2002). However, studies with the Atlantic coral *Siderastrea siderea* have shown that when monthly-resolved coral Sr/Ca is calibrated with in situ or local temperature records, the slopes and intercepts are virtually identical, within uncertainty estimates (DeLong et al., 2014; Flannery et al., 2017; Kuffner et al., 2017). *S. siderea* is relatively easy to micro-sample at monthly intervals compared to *Montastraea* corals that have a more complex skeletal structure with a deeper calyx that leads to mixing time intervals when micro-sampling (Leder et al., 1996; Sadler et al., 2014) resulting in a noisier geochemical signal (DeLong et al., 2011; Flannery et al., 2017).

The main source of Ba in seawater is river discharge that carries fine-grained suspended sediments with Ba attached that desorb at the river-seawater mixing zone (Edmond et al., 1978; Li and Chan, 1979; McCulloch et al., 2003; Moyer et al., 2012). Groundwater seepage in coastal environments can also contribute to Ba enrichment near the coast (Moore, 1997; Shaw et al., 1998). Barium concentration in coastal waters is, therefore, generally higher than in the open ocean. In the surface ocean, Ba concentration can increase in upwelling regions where colder nutrient-rich water comes to the surface increasing primary productivity (Carter et al., 2020; Lea et al., 1989; Reuer et al., 2003; Tudhope et al., 1996). Barium is not a nutrient but is removed from surface waters by adsorbing onto sinking organic matter that results in Ba depletion in the surface waters that is recycled at depth. Hence, barium in seawater reflects surface oceanic productivity resulting in a nutrient-like depth profile (Carter et al., 2020; Chow and Goldberg, 1960). Anthropogenic activities, such as catchment clearing, agricultural practices, and oil exploration, also affect Ba concentration in seawater depending on the source and location where these activities take place (Carriquiry and Horta-Puga, 2010; Deslarzes et al., 1995; McCulloch et al., 2003; Saha et al., 2018).

Several studies have used coral Ba/Ca as a proxy to reconstruct seawater Ba changes due to upwelling (up to 50 μmol/mol), river discharge and precipitation (up to 15 μmol/mol), land-use changes, mining, and oil drilling pollution (up to 9 μmol/mol; Table 1). The location of the coral is crucial to determine the environmental factors that influence the intensity and timing of the coral Ba/Ca signal. Existing measurements of coral Ba/Ca in the Pacific Ocean range from 2.5 to 15 μmol/mol whereas Caribbean Sea corals have a range of 3 to 11 μmol/mol. The higher values in the Caribbean are generally associated with upwelling (Reuer et al., 2003), yet coral Ba/Ca in the Gulf of Mexico has some of the highest coral Ba/Ca values published (Table 1). The study of Deslarzes et al. (1995) examined annually-resolved coral Ba/Ca (1910–1989) in a *Montastraea annularis* colony from WFGB that revealed a slight increase in coral Ba/Ca after the 1960s (range of 6 to 9.5 μmol/mol; Table 1). Those authors found a possible link to oil drilling muds that include barite ($BaSO_4$) but they suggest further evaluation with higher sampling resolution and better analytical precision are needed. A similar study conducted offshore of Veracruz, Mexico in the southwestern Gulf of Mexico (Fig. 1) examined annually-resolved coral Ba/Ca (1835–2000) in a *Montastraea faveolata* colony (Carriquiry and Horta-Puga, 2010). They found a similar mean shift in coral Ba/Ca (1.03 μmol/mol) occurring in 1965 when offshore Mexican oil exploration started along with land-use changes that increased sediment transport offshore. Both of those studies sampled their corals with annual resolution whereas seasonal or higher variability in coral Ba/Ca possibly driven by seasonal upwelling and freshwater floods are under-explored in the Atlantic region (Table 1). Understanding the seasonal variability coral Ba/Ca is important to ensure annually-resolved records are not biased by their sampling method and are not missing subannual environmental factors (e.g., productivity, upwelling, river discharge) driving coral Ba/Ca changes.

This study will examine subannual variations of coral Ba/Ca in a WFGB *S. siderea* colony for two-time intervals (1931–1944 and 1976–2004) before and during oil exploration and production. We explore the fidelity of the coral Ba/Ca determinations including analytical methodology, reproducibility, and coral sampling resolution. Monthly resolution allows us to investigate possible seasonal environmental forcing of coral Ba/Ca variability not previously detected with annual sampling resolution. The reproducibility of coral Ba/Ca within *S. siderea* corals has not been assessed in earlier studies whereas coral Sr/Ca reproducibility has been (DeLong et al., 2011; DeLong et al., 2016; DeLong et al., 2013; Flannery et al., 2017). In comparison to the previous Gulf of Mexico coral Ba/Ca studies (Deslarzes et al., 1995; Carriquiry and Horta-Puga, 2010), our study aims to provide insight into the environmental factors driving seawater Ba variability in the northern Gulf of Mexico and explore the extent oil exploration impacts on seawater Ba concentration. Our study design has selected an open ocean location far from river runoff and with little to no upwelling to isolate environmental factors in order to better understand changes in coral Ba/Ca and barium in seawater.

1.1. Study location

The Gulf of Mexico is a semi-enclosed ocean basin with a wide continental shelf where water depth is less than 200 m (Fig. 1). The Mississippi River system is the dominant source of freshwater to the Gulf of Mexico, which accounts for 64% of the total discharge into the Gulf (Darnell and Defenbaugh, 1990). Nutrient loading in the northern Gulf of Mexico leads to eutrophication and increased primary production in surface waters resulting in carbon loading on the seabed and hypoxia zones on the shelf (Rabalais et al., 2002). The mid-summer hypoxic zone west of the Mississippi River delta (>300 km away from the WFGB; Fig. 1) is among the largest in the world where bottom water anoxia leads to releasing toxic hydrogen sulfide from the sediments (Rabalais and Turner, 2001). The Loop Current brings warm and salty Caribbean water into the Gulf of Mexico and exits through the Straits of Florida to form the Gulf Stream (Walker, 2005). In the northwestern Gulf of

Table 1
Summary of coral Ba/Ca studies.

Species	Location(s)	Coral Ba/Ca[a] (μmol/mol)	Local processes	Resolution	Instrument[b]	Precision[c]	Reference
Porites spp.	Northeast Madagascar	~7.5	–	~monthly	ICP-MS	2.2%	Nagtegaal et al., 2012
Porites spp.	Antongil Bay, Madagascar	6.75 ± 0.78 6.05 ± 0.75	Runoff Runoff	Monthly Subweekly	HR-ICP-MS LA-ICP-MS	6% 4.3%	Grove et al., 2013, 2012
Porites	Malindi Coral Reef, Kenya	~3 to 50	Runoff	Subweekly	LA-ICP-MS	**	Fleitmann et al., 2007
Porites	Sodwana Bay, South Africa	<0.003 no units	–	Biweekly	Ion microprobe	1.5% Ba	Hart and Cohen, 1996
Porites spp.	Coral Gardens Reef, Red Sea	~4.1 to 10.7	Wind driven dust	~2 weeks	ICP-MS	2.4%	Bryan et al., 2019
Porites	Marbat and Wadi Ayn, Oman	up to 17	Upwelling	Monthly	ICP-MS	0.8%	Tudhope et al., 1996
Porites spp.	Cygnet Bay, Kimberley region, Northwestern Australia	4.1 to 7.0	Runoff	Subannual	Q-ICP-MS	±0.205	Chen et al., 2020
Porites spp.	Thailand, Singapore, and Taiwan	1.8 to 161.8 includes tissue layer	Runoff and typhoons	Weekly	LA-ICP-MS	**	Moynihan et al., 2021
Porites lutea	Pulau Kusu and Pulau Hantu, Singapore	~2 to 14	Runoff	Monthly	LA-ICP-MS	3.7%	Tanzil et al., 2019
Porites sp.	Kusu Island, Singapore	~2.5 to 15	–	~2 weeks	ICP-OES ICP-MS	±0.38 ±0.33	Cantarero et al., 2017
Porites spp.	Luzon Strait, South China Sea	2 to 3.5	Runoff	Annual	MC-ICP-MS	3%	Liu et al., 2019
P. lutea	Hainan Island, South China Sea	~3 to 10	Runoff	~2 per year	ICP-OES	3%	Jiang et al., 2017
Porites	Daya Bay, South China Sea	~6 to 15	Stress-low SST	~2 months	ICP-AES	3%	Chen et al., 2011
Porites lobata	Lanyu Islet, Taiwan	1.71 to 4.28	Runoff	~3 months	SF-ICP-MS	0.6%	Yu et al., 2015
Porites sp. (modern)	Shiraho Reef, Ishigaki Island, Japan	3.39 to 4.16	Runoff	~2 months	ICP-AES	0.3%	Sowa et al., 2014
Porites sp. (fossil)	Nagura Bay, Ishigaki Island, Japan	1.78 to 11.5	Runoff	Monthly	ICP-AES	0.3%	
Porites sp. JCp-1	Ishigaki Island, Ryukyu Islands, Japan	7.465 ± 0.655	NA	NA	multiple instruments	NA	Hathorne et al., 2013
P. lobata	Okinotori Island, Japan	5 to 14	Upwelling	~10 days	LA-ICP-MS	**	Yamazaki et al., 2011
Porites	Sumiyo Bay, Japan	~4	Runoff	0.3 month	ICP-OES	±0.18 (2.24%)	Ito et al., 2020
P. lobata	Shirigai Bay, Japan	~4 to 5.5	Upwelling	Subweekly	LA-ICP-MS	4.3%	Fallon et al., 1999
Porites	Papua New Guinea	3.5 to 4.5	Runoff	~2 months	ICP-MS	0.8%	Tudhope et al., 1997
Porites	New Ireland, Papua New Guinea	~4 to 50	Upwelling	Monthly	LA-ICP-MS	**	Alibert and Kinsley, 2008
P. lutea	Cow and Calf Island, Orpheus Island, King Reef and Pandora Reef, Australia	~3 to 18	Runoff	~Weekly	LA-ICP-MS	3.7%	Sinclair, 2005; Sinclair and McCulloch, 2004
Porites sp.	Great Keppel Island, Australia	~3.5 to 7.0	Runoff	Subannual	ICP-MS	0.46%, 1.0%	Saha et al., 2018, 2019
Porites spp.	Pandora Reef, Australia	3 to 12	Runoff	Subannual	LA-ICP-MS	±0.04 (2σ, Ba)	Alibert et al., 2003
Porites spp.	Great Barrier Reef, Australia	4 to 13	Runoff	Subannual	LA-ICP-MS	**	Lewis et al., 2018
Porites spp.	Frankland Islands, Great Barrier Reef, Australia	1.90 to 10.10	Runoff	Subannual	ICP-MS	<5%	Leonard et al., 2019
Porites	Great Barrier Reef, Australia	4.3 ± 1.9	Runoff, upwelling	Subannual	LA-ICP-MS	4.3%	Walther et al., 2013
Porites	Great Barrier Reef, Australia	~4 to 20	Runoff	~Weekly	LA-ICP-MS	**	Wyndham et al., 2004
Porites	Southern Great Barrier Reef, Australia	4.98 ± 0.63	Runoff	~Weekly	LA-ICP-MS	**	Jupiter et al., 2008
Porites spp.	Havannah Reef, Australia	3 to 15	Runoff	~Weekly	LA-ICP-MS	**	McCulloch et al., 2003
Porites sp.	Arlington Reef, Australia	~2.3 to 6.8	Runoff	Annual	ICP-AES	1–3%	Wei et al., 2009
P. lutea	Amédee Island, New Caledonia	3.6 to 9.5	–	Monthly	ICP-MS	0.60%	Quinn and Sampson, 2002
P. lobata (fossil)	Vata-Ricaudy, New Caledonia	1.3 to 5.2	Upwelling	Monthly	ICP-MS	±0.18 (2σ)	Montaggioni et al., 2006
Porites spp.	Uitoé, New Caledonia	~2.5 to 12	Upwelling	Subannual	ICP-MS	<2%	Ourbak et al., 2006
P. lobata	One Ali'I reef, Moloka'i, Hawai'i	4.19 to 10.19	Groundwater discharge, runoff	~Weekly	LA-ICP-MS	4–13%	Prouty et al., 2010
Pavona clavus	Punta Pitt, Galapagos	~3.9 to 4.9	Upwelling	~3 months	ICP-MS	1%	Lea et al., 1989; Shen et al., 1992
P. lobata	Gulf of Panama	4 to 8	Upwelling	<1 year	HR-ICP-MS	5.8%	LaVigne et al., 2016
Pavona gigantea	Gulf of Panama	4.8 to 6.5					
P. clavus	Gulf of Panama	4 to 6.5					
Pocillopora damicornis	Gulf of Panama	~1 to 9.5	Upwelling	~1–2 years	ICP-OES	0.19%	Toth et al., 2015
Montastraea annularis	Barbados	~5	Runoff	~3 months	GF-AAS	5–10%	Shen and Sanford, 1990
Diploria strigosa	Buccoo Reef, Tobago	~5		Annual			
M. annularis	Barbados	6.4 ± 0.4 Ba only		Bulk	DCP	3%	Pingitore et al., 1989
Acropora palmata		9.3 ± 2.10 Ba only					
M. annularis	Isla Tortuga, Venezuela	~4.2 to 5.8	Upwelling	~2 months	ICP-MS	**	Reuer et al., 2003
Siderastrea siderea	Isla Tortuga, Venezuela	~6.5 to 11	Upwelling	~6 months	ICP-MS	**	
Montastraea faveolata	Fajardo, Puerto Rico	3.87 to ~5.20	Runoff	Subannual	LA-ICP-MS	10%	Moyer et al., 2012

(*continued on next page*)

Table 1 (*continued*)

Species	Location(s)	Coral Ba/Ca[a] (μmol/mol)	Local processes	Resolution	Instrument[b]	Precision[c]	Reference
Ceratoporella nicholsoni (sclerosponge)	Tongue of the Ocean, Bahamas	3.4 ± 0.25	Open ocean	~10 per year	LA-ICP-MS	**	Rosenheim et al., 2005
		3.72 ± 0.27	Open ocean	8 per year	ICP-OES	**	
C. nicholsoni (sclerosponge)	Pear Tree Bottom, Jamaica	1.29 ± 0.034	Groundwater?	~7 per year	LA-ICP-MS	**	
		3.87 ± 0.27	Groundwater?	~yearly	ICP-OES	**	
M. faveolata	Mesoamerican Reef	3.43 ± 0.226	Runoff	Annual	HR-SF-ICP-MS	**	Carilli et al., 2009
M. annularis	Punta Nizuc Reef, Mexico	5.90 ± 0.56	Coastal runoff, ground water	Annual	ICP-OES	~4.0%	Horta-Puga and Carriquiry, 2012
A. palmata	Puerto Morelos Reef, Yucatan Peninsula, Mexico	18 ± 13.9 Ba only	Groundwater seepage	Bulk	ICP-MS	<1% Ba	Kasper-Zubillaga et al., 2014
Acropora cervicornis		14.33 ± 5.22 Ba only					
Gorgonia ventalina		11.33 ± 3.63 Ba only					
Siderastrea radians	Florida Bay, Florida	~5.48	Runoff	4–6 months	ICP-MS	**	Swart et al., 1999
M. faveolata	Veracruz, Gulf of Mexico	7.76 ± 0.83	Upwelling, runoff, and oil production	Annual	ICP-OES	~4.0%	Carriquiry and Horta-Puga, 2010
M. annularis	West Flower Garden Bank, Gulf of Mexico	7.6 ± 0.1 (~6.0 to 9.1)	Oil production	Annual	DCP	8% Ba, 7% Ca	Deslarzes et al., 1995; Deslarzes, 1992
S. siderea	West Flower Garden Bank, Gulf of Mexico	11.97 ± 0.21 (4.46 to 28.52)	Oil production	Subannual	ICP-OES	±0.12 (1.51%)	This study

[a] Reported as range and/or mean with ±1σ unless otherwise noted.
[b] Instrument abbreviations are inductively coupled plasma optical emission spectrometer (ICP-OES), inductively coupled plasma atomic emission spectrometer (ICP-AES), inductively coupled plasma mass spectrometer (ICP-MS), high resolution ICP-MS (HR-ICP-MS), quadrupole ICP-MS (Q-ICP-MS), multi-collector ICP-MS (MC-ICP-MS), laser ablation ICP-MS (LA-ICP-MS), sector field ICP-MS (SF-ICP-MS), graphite furnace atomic absorption spectroscopy (GF-AAS), and directly coupled plasma (DCP).
[c] Ba/Ca precision as reported by original authors is ± μmol/mol or % relative standard deviation (RSD) 1σ unless otherwise noted.
** Indicates precision was not reported in the publication.

Mexico, northeasterly winds prevail in the winter and are replaced by southwesterly winds in the summer. The wind reversal that occurs in the springtime generates shallow coastal upwelling (~180 km away from the WFGB) along the southern Texas and northern Mexican coasts (Walker, 2005). The Gulf of Mexico frequently experiences hurricanes that can mix colder deep water with the surface water resulting in surface enrichment of nutrients days to a week after a storm's passage (Walker et al., 2005).

2. Methods

A 1.74 m long cylindrical core (in five sections) from a *S. siderea* coral colony in WFGB (27° 52′ N, 93° 49′ W) was collected in May 2005 at a depth of 23.8 m by a team of divers from Flower Garden Banks National Marine Sanctuary and Texas A&M University. The team used an underwater hydraulic drill with a 4-inch diameter diamond-tipped drill bit and drilled vertically down from the top center of the coral colony. Slabs of ~8 mm thickness were cut from the core along lines that produced transects of the extending corallites along their growth trajectories with their synapticulothecal walls parallel to the slab surface; the optimal sampling location for developing geochemical histories for this coral species (DeLong et al., 2016). Core section 05WFGB3-1-A was cut into quarter sections to achieve suitable slabs for geochemical sampling. The slabs were cleaned with a Branson 400 sonifier digital ultrasonic cell disruptor using deionized water to remove organic matter, dust, and cuttings. This study focuses on the top core section 05WFGB3-1-A that broke into two pieces after slabbing (labeled 05WFGB3-1-A1 and 05WFGB3-1-A2; Fig. 2). Digital X-radiographs of the coral slabs were taken at the Louisiana State University (LSU) Forensic Anthropology and Computer Enhancement Services Laboratory and were exposed at 48 kV for 0.4 s and then processed by an Agfa CR35-X digital processor (Fig. 2). Coral slabs were scanned on an Epson Expression 10000 XL scanner at 1200 dpi and then overlaid with X-radiographs in Adobe Photoshop. The distance between growth band couplets in the X-radiographs were measured for each year to determine the micro-sampling interval (0.4 mm) for monthly sampling resolution.

An automated tri-axial micromill system (Taig Micromill with SuperCAM software from Supertech and Associates, Phoenix, Arizona) was used to extract continuous micro-samples from the coral slab surface using a box (0.4 mm × 0.4 mm) milling path with a 0.4 mm forward increment and a 1.0 mm sampling depth using a 1.0 mm diameter dental drill bit producing ~500 μg of coral powder (Fig. 2). Divots (1.5 mm deep) were made at every 12th sample as markers to assist in assigning time to the coral geochemistry. To assess reproducibility, three parallel sampling paths were micro-milled (2015, 2018, and 2019 paths; Fig. 2) and a fourth path on the opposing side (2020 path) in 05WFGB3-1-A1. All paths in 05WFGB3-1-A2 were micro-milled on the same side. Sampling paths were shifted purposely to avoid the columella or when the synapticulothecal wall structure was suboptimal or discontinuous due to the synapticulothecal walls bifurcating, or corallites were found to be at an angle to the slab surface (DeLong et al., 2016). New paths were overlapped at least by a year with the previous path to align them with each other and to check reproducibility.

A PerkinElmer 8300 inductively coupled plasma optical emission spectrometer (ICP-OES) in the LSU PAST Laboratory was used to determine coral elemental ratios (Sr/Ca, Mg/Ca, and Ba/Ca) for all paths except path 2015 (Sr/Ca and Mg/Ca) that was measured at the University of Maryland Center for Environmental Science Chesapeake Biological Laboratory campus (UMCES-CBL) with the same ICP-OES model and methods. An aliquot of each micro-sample was weighed using a microbalance (±1 μg) so that the final calcium concentration was ~20 mg/L when dissolved in 2% trace metal grade HNO_3. The ICP-OES was optimized to measure the peak intensity area of spectral wavelengths for each element (Sr 421.552 nm; Ca 315.887 nm, 317.933 nm, and 422.673 nm; Mg 279.553 nm; Ba: 455.403 nm and 493.408 nm). The less sensitive radial torch view was used for Ca 422.673 nm and Sr 421.552 nm and the other wavelengths used the axial window for analytes with a lower concentration in corals (Mg and Ba). An internal gravimetric standard (IGS) was prepared by mixing aliquots of ultrapure solution standards (Ca, Sr, Mg, and Ba) to produce a typical coral concentration and was measured before and after each sample to correct for instrumental drift (Schrag, 1999). A homogenized powder from a *Porites*

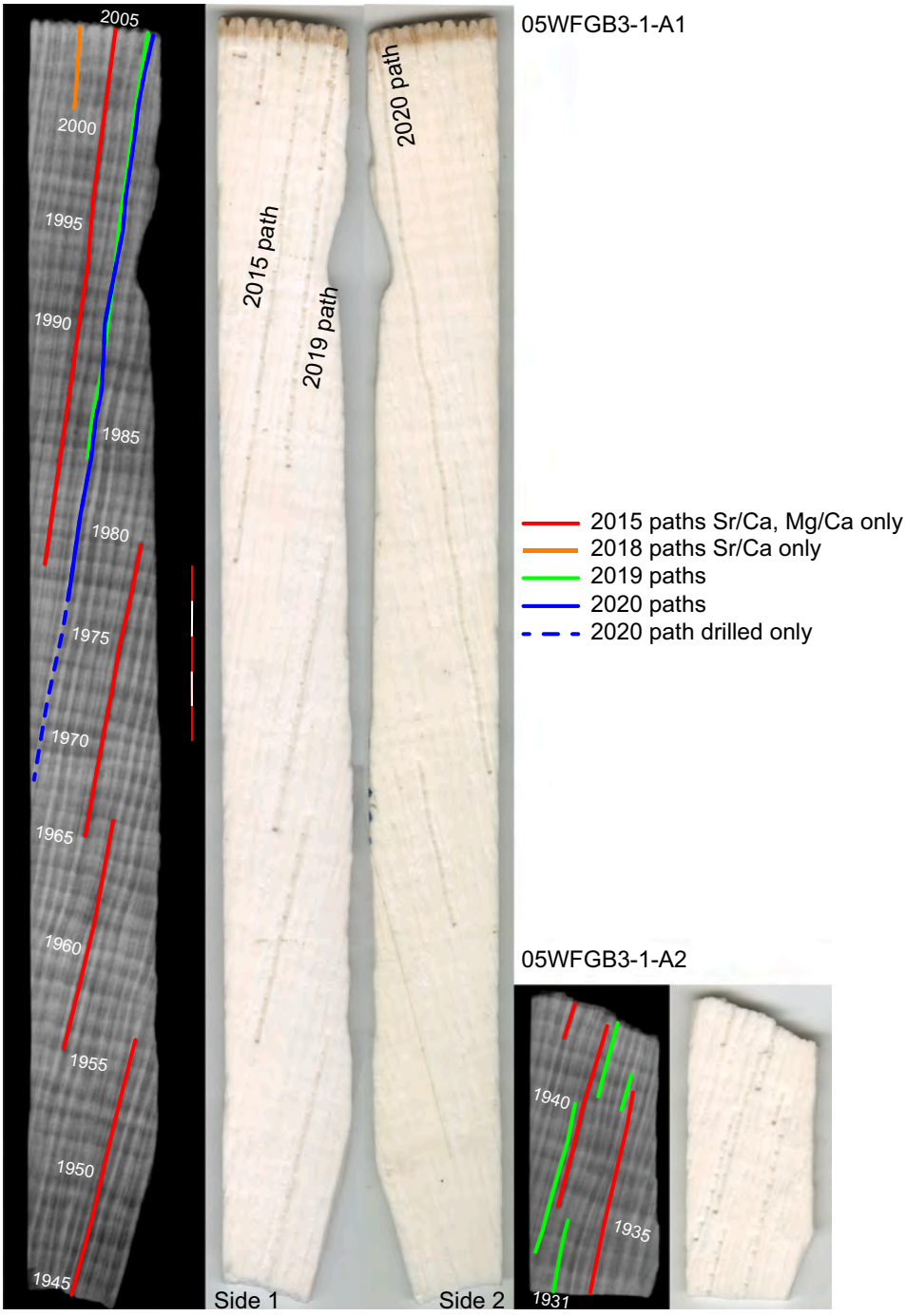

Fig. 2. X-radiographs and scans of the *S. siderea* coral slabs. Years are noted starting from the core top (2005) with sampling paths locations. Scale bar is 50 mm with 10 mm intervals.

lutea coral (PL) was dissolved in bulk and used as a matrix-match external standard analyzed after every fifth coral sample. Highly accurate and precise values for Sr/Ca, Mg/Ca, and Ba/Ca for PL and IGS were determined by multi-collector inductively coupled plasma mass spectrometer (MC-ICP-MS) in the High-Precision Mass Spectrometry and Environmental Change (HISPEC) Laboratory in the Department of Geosciences at National Taiwan University (Lo et al., 2014). The international coral reference JCp-1 (Hathorne et al., 2013; Okai et al., 2002) is a coral powder that is weighed out for each run and was measured as a second external matrix-match reference at the beginning and end of an analysis run with 100 coral samples and the beginning of an analysis run with 50 coral samples. Precision and accuracy for the LSU laboratory are reported in Fig. 3 and for LSU and UMCES-CBL laboratories in Supplementary Tables 1 and 2.

Time assignment for each coral Sr/Ca path was performed using Analyseries software (Paillard et al., 1996) with a monthly sea surface temperature (SST) time series (ERSST version 3b for the 2° grid box centered on WFGB, 28°N, 94°W; WFGB-SST) (Reynolds et al., 2002; Reynolds and Smith, 1994). Coral Sr/Ca maxima and minima were assigned to the coldest (i.e., winter) and warmest (i.e., summer) months of the annual sea surface temperature (SST) cycle, respectively. Corals may grow faster in summer when compared with winter; therefore, time assignment using only summer and winter months may be biased towards the season with more growth. Therefore, additional ties were

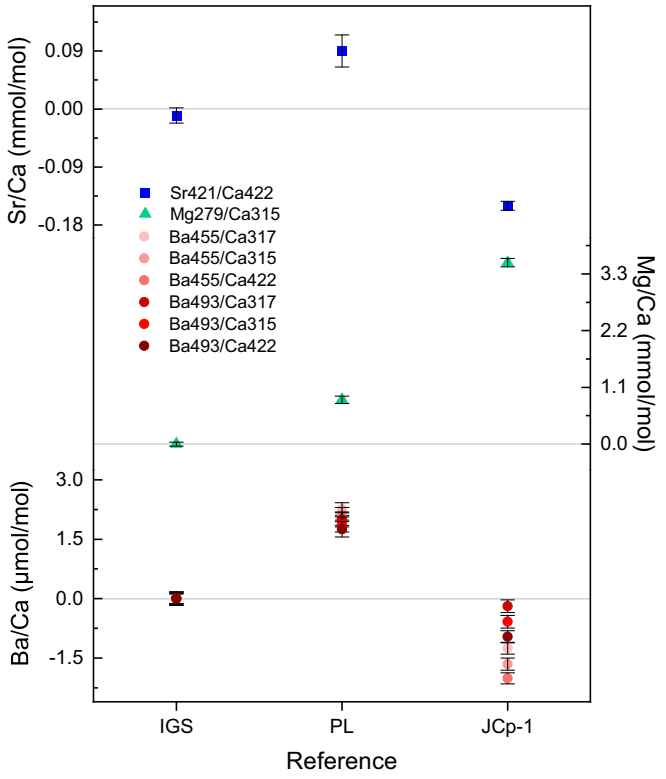

Fig. 3. Precision and accuracy of coral Sr/Ca, Mg/Ca, and Ba/Ca for LSU. IGS has been corrected to the value determined by the HISPEC Laboratory following Schrag (1999).

placed in mid-spring and mid-autumn in Analyseries to further constrain the annual coral Sr/Ca cycles to SST. The time assigned to the coral Sr/Ca paths were applied to the respective coral Mg/Ca and Ba/Ca records and each was linearly interpolated to even monthly time intervals in Analyseries to facilitate comparison with monthly climatological records. The master chronology for 05WFGB3-1-A was developed by counting Sr/Ca annual cycles from the top of the core (2005) that were cross-checked with density bands in the X-radiographs (Fig. 2). A coral sample taken below the 05WFGB3-1-A2 core section was dated by using high precision ^{230}Th dating technique (Shen et al., 2003; Shen et al., 2008) to confirm the chronology. The uranium-thorium analysis was conducted with a Thermo Electron Neptune MC-ICP-MS (Cheng et al., 2013; Shen et al., 2012) in the HISPEC Laboratory. To generate the master geochemical time series, contemporaneous samples from each path were averaged together and the standard error of the mean was determined for each master monthly coral Sr/Ca value that will be used to determine the weights for weighted least-squares linear regression (Section 3.2). The annual linear extension (mm) was determined by the distance between coral Sr/Ca maxima (i.e., winter values). A 5% significance level was assumed for all statistical analyses.

3. Results

Core section 05WFGB3-1-A1 spans 60 years from 1945 to 2005.04 and 05WFGB3-1-A2 spans 12.58 years from 1931.71 to 1944.29 (Fig. 2). Coral Sr/Ca from 1931.71 to 2005 was used to build a continuous chronology; however, this study will focus on the two intervals for which coral Ba/Ca measurements were completed. Years determined by coral Sr/Ca cycles and the X-radiographs agree with the ^{230}Th dating results (±2.4 years, 2σ; Supplementary Table 3).

All six Ba/Ca wavelength combinations are evaluated and compared for precision and accuracy for IGS, PL, and JCp-1 (Fig. 3, Supplementary Table 2). The average precision value for the three Ba 455 nm/Ca combinations are ~25% lower for IGS, ~16% lower for PL, and ~6% lower for JCp-1 (i.e., more precise) when compared with the precisions determined for the three Ba 493 nm/Ca combinations. Out of all wavelength combinations, Ba 455 nm/Ca 317 nm has the smallest IGS precision value whereas Ba 455 nm/Ca 422 nm has the smallest JCp-1 precision. The average accuracy value for the three combinations of Ba 493 nm/Ca is ~12% lower for PL and ~65% lower for JCp-1 (i.e., more accurate) when compared with the average accuracy of three Ba 455 nm/Ca combinations. Out of all wavelength combinations, JCp-1 accuracy for Ba 493 nm/Ca 317 nm has the smallest value. This study will use Ba 455 nm/Ca 317 nm since this wavelength combination had an acceptable accuracy and precision and we have a complete Ba/Ca record. Discrepancies among the six Ba/Ca wavelengths combinations for all coral determinations are less than the lowest analytical precision (<±0.24 μmol/mol, 2σ; Supplementary Table 2). The previous WFGB study (Deslarzes et al., 1995) used a Directly Coupled Plasma Spectrometer with an analytical precision almost as large as their coral Ba/Ca signal (Table 1). One of the earliest coral Ba/Ca studies to use an ICP-OES was in the Gulf of Mexico (Carriquiry and Horta-Puga, 2010) (Table 1) and that study demonstrated improved analytical precision.

A summary of the geochemical results for the two-time intervals is provided in Table 2. In the tissue layer at the top of the core (0–12 mm; Fig. 4), monthly coral Ba/Ca values range from ~50 to 800 μmol/mol and coral Mg/Ca is anomalously high due to the presence of organic matter in the tissue layer and therefore samples in the tissue layer are excluded from the rest of this study, which is standard practice. The average monthly coral Sr/Ca for 05WFGB3-1-A1 and 05WFGB3-1-A2 differ by 0.026 mmol/mol or ~0.6 °C, which is close to the observed SST difference for WFGB-SST (Reynolds and Smith, 1994) for these two-time intervals. Monthly coral Sr/Ca negatively correlates with monthly coral Mg/Ca ($r = -0.87$, $n = 332$) and monthly coral Ba/Ca ($r = -0.42$, $n = 333$). Coral Mg/Ca data are included for completeness but will not be discussed further. Correlation is not significant between annual linear extension and annual average coral Sr/Ca or coral Ba/Ca for 05WFGB3-1 (Supplementary Table 4).

3.1. Reproducibility

Intra-coral reproducibility for coral Sr/Ca and coral Ba/Ca variations are assessed by pairwise comparison among the sampling paths in 05WFGB3-1-A1 (Figs. 2 and 4). Monthly coral Sr/Ca significantly correlates among all paths (Table 3). The average differences in contemporaneous coral Sr/Ca values between path 2019 and path 2015 is less than analytical precision, but the differences between path 2019 and path 2020, and path 2015 and path 2020 are greater than the ±2σ analytical precision. Path 2018 is just four years long and agrees with path 2020 (Fig. 4). Microscopic examination of the beginning of path 2015 and path 2019 (2000–2005) reveals suboptimal corallite orientation (DeLong et al., 2016). Both paths agree within ±2σ analytical precision with path 2020 before the year 2000 when the corallites are optimally aligned in the sampling path (Fig. 4). These suboptimal sections are excluded from further analysis and from the master geochemical time series (Fig. 5). The average of the absolute differences, which is the discrepancy between two values for any given month (DeLong et al., 2014; DeLong et al., 2016; DeLong et al., 2007), for coral Sr/Ca is 0.050 mmol/mol for 1977.63 to 2000.13 and is close to the IGS 2σ precision range (0.048 mmol/mol), similar to other reproducibility studies for *S. siderea* (DeLong et al., 2011; DeLong et al., 2016). The coral Sr/Ca values determined by different labs (LSU path 2018, path 2019, and path 2020) and (UMCES-CBL path 2015) similarly agree within ±2σ analytical precision for optimally sampled portions (1977.63–2000.13) of those paths. Coral Ba/Ca from path 2019 and path 2020 are significantly correlated and the mean difference of 0.29 μmol/mol is not significant (Table 3). The coral Ba/Ca variations are generally well-reproduced in mean value and variability, even when sampling opposing sides of the coral slab, with the largest differences occurring in

Table 2
Summary of monthly-resolved elemental ratios for 05WFGB3-1.

	05WFGB3-1-A1 (1976–2004)[a]			05WFGB3-1-A2 (1931–1944)		
	Sr/Ca (mmol/mol)	Mg/Ca (mmol/mol)	Ba/Ca (μmol/mol)	Sr/Ca (mmol/mol)	Mg/Ca (mmol/mol)	Ba/Ca (μmol/mol)
Average	8.912	4.646	12.52	8.938	4.540	10.76
Median	8.909	4.644	11.46	8.931	4.538	9.56
Standard deviation	0.139	0.372	4.98	0.134	0.325	3.79
Variance	0.019	0.138	24.83	0.018	0.106	14.35
Maximum	9.210	6.438	28.52	9.194	5.832	27.62
Minimum	8.618	3.744	4.46	8.667	3.967	6.07
# of observations	343	332	333	153	153	153
Average annual linear extension	5.4 ± 0.3 mm			6.2 ± 0.3 mm		

[a] Values from the tissue layer (0–12 mm) are excluded for Mg/Ca and Ba/Ca.

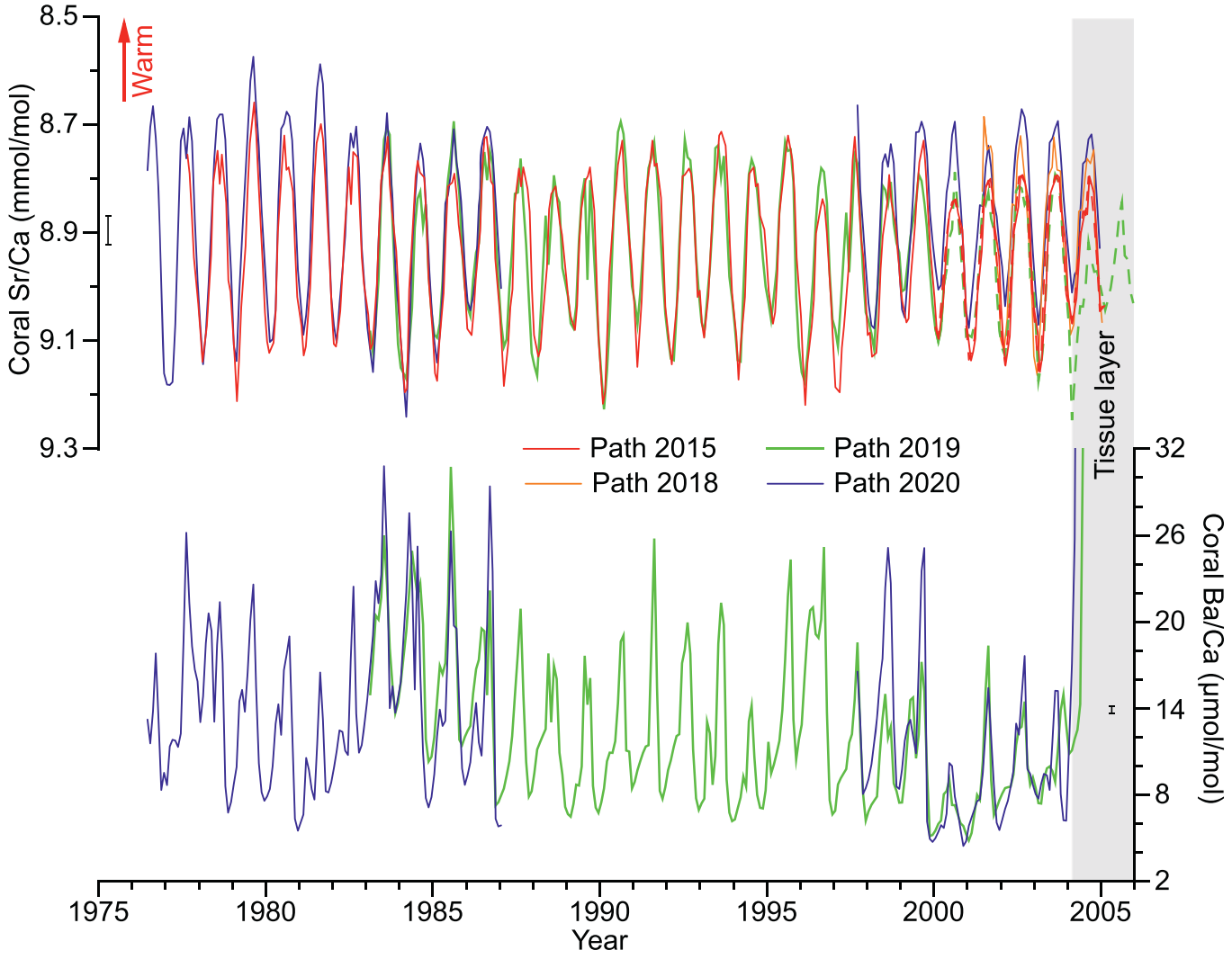

Fig. 4. Reproducibility of monthly coral Sr/Ca (top) and coral Ba/Ca (bottom) variations. Coral Sr/Ca is inverted to depict warmer temperatures as up. The shaded area denotes the tissue layer where coral Ba/Ca values >32 μmol/mol are not plotted. Dashed portions of paths are suboptimal and are excluded from further analysis. Error bars are analytical precision (2σ).

the seasonally higher coral Ba/Ca values (Fig. 4). This result suggests intra-coral Ba/Ca is reproducible similar to coral Sr/Ca.

3.2. Coral Sr/Ca-temperature calibration

The monthly master coral Sr/Ca is calibrated to the monthly mean temperature determined from daily reef temperatures (20 m water depth) reporteded by Johnston et al. (2020) at WFGB spanning 1986–2004 (Fig. 6). The master coral Sr/Ca and reef temperature are significantly correlated ($r = -0.89$, $n = 140$). Weighted least square regression (DeLong et al., 2014; York and Evensen, 2004) was used to determine the calibration equation (Eq. (1)) using the standard error of the mean for each month as weights for reef temperature and coral Sr/Ca resulting in a root mean square error of ±0.58 °C (1σ).

$$\text{Coral Sr/Ca (mmol/mol)} = -0.042\,(\pm 0.0002) \times \text{SST (°C)} + 9.945\,(\pm 0.005) \quad (1)$$

Table 3
Summary of reproducibility tests for coral Sr/Ca and coral Ba/Ca (1977.63–2000.13).

Paths	Elemental ratio	Correlation		*t*-test			
		r^a	*p*-value	Mean difference	*t*	*t* critical	n^b
Paths 2015 & 2019	Sr/Ca	0.91	7.59×10^{-83}	0.003 mmol/mol	0.221	1.966	205
Paths 2019 & 2020	Sr/Ca	0.93	5.97×10^{-39}	0.043 mmol/mol	2.166	1.973	90
Paths 2015 & 2020	Sr/Ca	0.95	3.65×10^{-80}	0.051 mmol/mol	2.985	1.968	144
Paths 2019 & 2020	Ba/Ca	0.80	2.09×10^{-21}	0.29 μmol/mol	0.306	1.973	90

[a] Pearson's correlation coefficient *r*.
[b] Number of contemporaneous observations in paths.

3.3. Coral Ba/Ca variability

There is a significant increase in the mean coral Ba/Ca of 1.76 μmol/mol between the time intervals examined (1931–1944 and 1976–2004; Fig. 7). The average coral Ba/Ca difference between June and August (summer increase) is 6.52 μmol/mol in 1931–1944 and 5.00 μmol/mol in 1976–2004, which is a less pronounced summer increase in the 1976–2004 interval. Additionally, coral Ba/Ca seasonality has increased by 2.42 μmol/mol (~18%) between these time intervals. For 1976–2004, the mean coral Ba/Ca winter minima have increased by 6.2%, and the mean summer maxima have increased by 13.75% when compared to the 1931–1944 time interval. Subannual variations in coral Ba/Ca reveal different annual cycles for each time interval with summer maxima and winter minima that are ~180° out of phase with coral Sr/Ca (Fig. 7).

4. Discussion

4.1. Assessing coral Ba/Ca precision and accuracy

The wavelength combination we selected, Ba 455 nm/Ca 317 nm, based on a combination of precision and accuracy assessments (Supplementary Table 2), are the same wavelengths used by Cantarero et al. (2017) and our precision is comparatively better although we did not

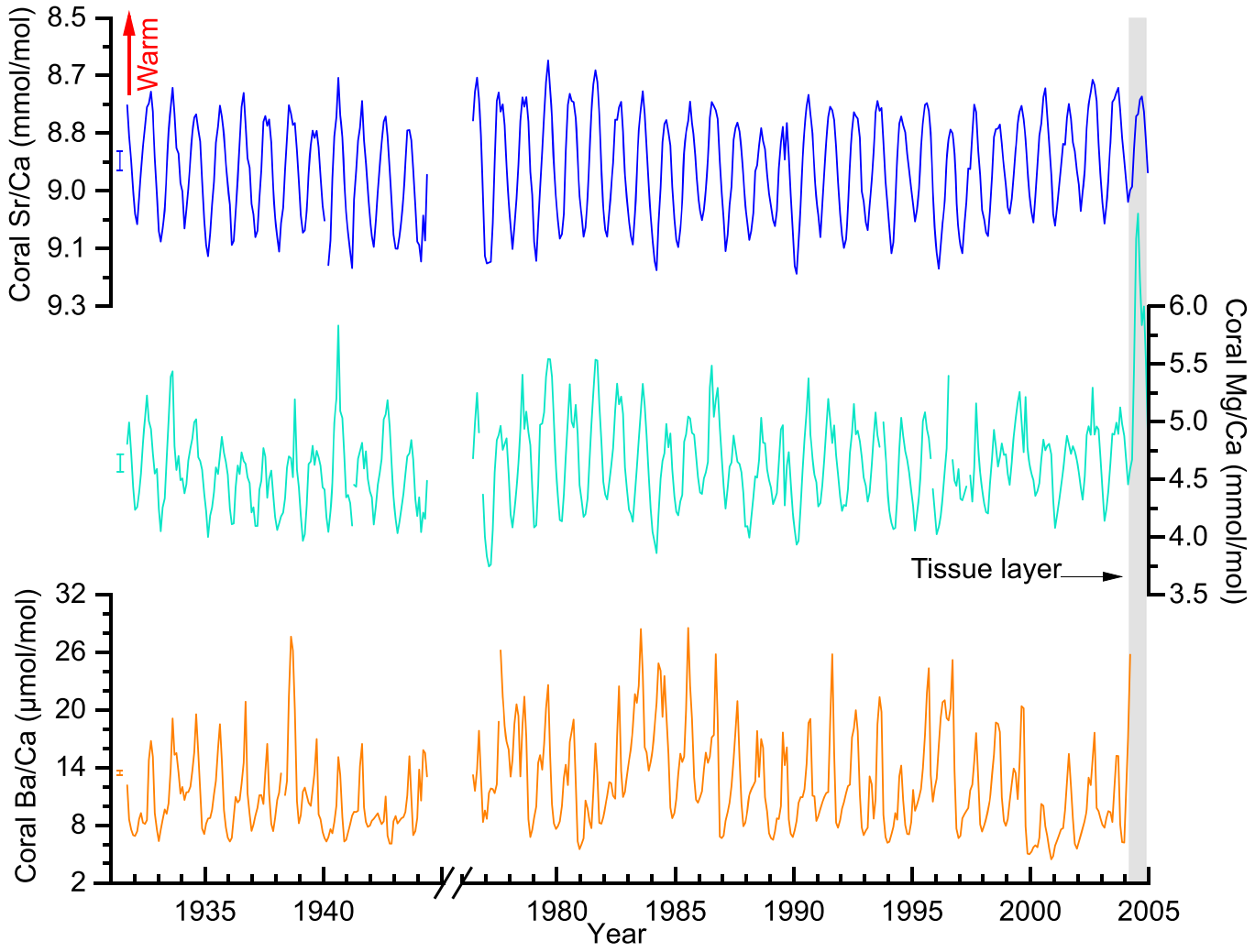

Fig. 5. Master time series for monthly coral Sr/Ca (blue), Mg/Ca (aqua), and Ba/Ca (orange) for 1931.71 to 1944.29 and 1976.46–2004.96. Coral Sr/Ca is inverted to depict warmer temperatures as up. Error bars are analytical precision (2σ). (For interpretation of the references to colour in this figure legend, the reader is referred to the web version of this article.)

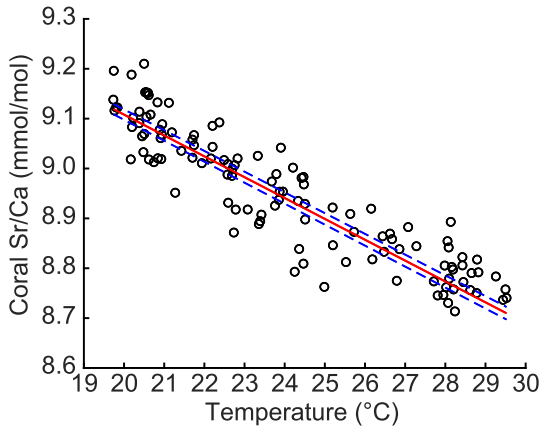

Fig. 6. Scatter plot of monthly coral Sr/Ca and monthly reef temperatures (black circles). The solid red line is the linear regression line and the dashed blue line is the 95% confidence belt. (For interpretation of the references to colour in this figure legend, the reader is referred to the web version of this article.)

have as many JCp-1 measurements ($n = 13$). An interlaboratory study (Hathorne et al., 2013) reported element/Ca values for JCp-1 measured by 21 laboratories and 10 of those laboratories returned values for coral Ba/Ca with at least three of those laboratories using an ICP-OES or ICP-AES (both use the same technology). That study reports an interlaboratory robust standard deviation for coral Ba/Ca as ±0.655 μmol/mol (1σ), which is about five times greater than our JCp-1 Ba/Ca precision. One ICP-OES laboratory returned a JCp-1 Ba/Ca value that was lower than the rest and was excluded whereas the other ICP-OES laboratories had Ba/Ca standard deviations values similar to the ICP-MS laboratories, which are presumably more precise and accurate. The study of Cantarero et al. (2017) compared their internal coral standard results for coral Ba/Ca determined with ICP-OES and ICP-MS and found an offset (1.14 ratio factor). Similar differences between ICP-OES and ICP-MS were noted for coral Sr/Ca (Ourbak et al., 2006) and sclerosponge Ba/Ca (Rosenheim et al., 2005) yet the interlaboratory experiment of Hathorne et al. (2013) does not show evidence of an instrumental bias. Furthermore, our study and Cantarero et al. (2017) both have average JCp-1 Ba/Ca values less than the Hathorne et al. (2013) reported robust average of 7.465 μmol/mol that is based on nine laboratories with analytical precisions varying by an order of magnitude (±1.30 to ±0.1 μmol/mol, 2σ). We suggest this interlaboratory average may not reflect the "true" Ba/Ca value for JCp-1. As more laboratories analyze coral Ba/Ca, especially with ICP-OES (Table 1), a reassessment of JCp-1 for Ba/Ca may be warranted. We further suggest accuracy assessment for coral Ba/Ca should use two or more external coral references for comparison (e.g., PL and JCp-1). Some studies may use the Hathorne et al. (2013) JCp-1 robust average for their instrumental drift correction (de Villiers et al., 2002; Schrag, 1999) and we advise against this practice for coral Ba/Ca determinations since the interlaboratory study's average value may not be the true value.

4.2. Coral geochemistry fidelity

The linear extension per year is greater than 2.0 mm, the growth effect threshold for *S. siderea* (DeLong et al., 2016; Kuffner et al., 2017), thus no growth effects for coral Sr/Ca or sampling artifacts resulting in reduced seasonal cycles were found. The average annual linear extension for this study (Supplementary Table 4) is comparable to that of observed in other *S. siderea* in the Gulf of Mexico (DeLong et al., 2014;

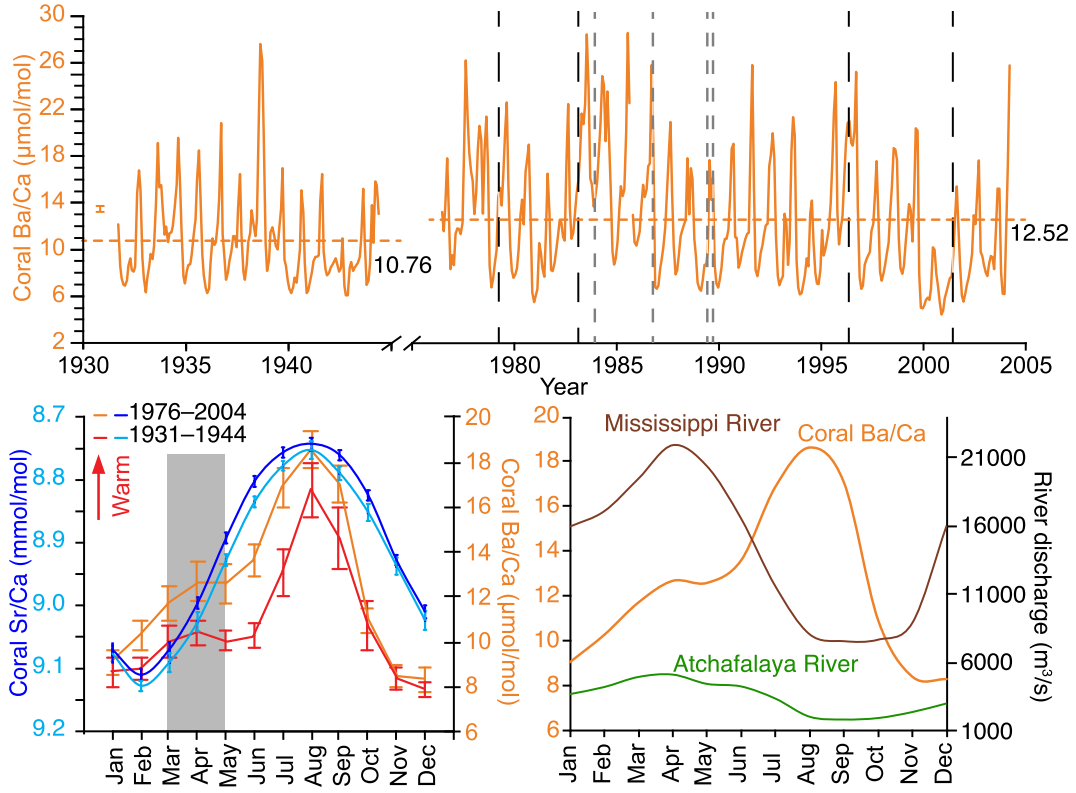

Fig. 7. Monthly coral Ba/Ca for 1931–1944 and 1976–2004 (top). The dotted orange lines are the means for each time interval. Error bar is analytical precision (2σ). Black and grey lines indicate major flood events in the lower Mississippi River (National Weather Service, 2019) and hurricanes passing near the WFGB (Landsea and Franklin, 2013), respectively. Average monthly coral Ba/Ca and Sr/Ca for the two-time intervals (bottom left) where the grey box indicates a springtime slight increase in coral Ba/Ca. Error bars are standard error of the mean. Average river discharge by months and coral Ba/Ca (bottom right); adapted from Wagner and Slowey (2011).

Flannery et al., 2017; Kuffner et al., 2017) and the Caribbean (Reich et al., 2013). Conversely, Saenger et al. (2009) had a *S. siderea* coral with an annual linear extension averaging 2.0 mm, thus ~50% of the years were below the growth effect threshold (DeLong et al., 2016; Kuffner et al., 2017) and perhaps the slower growth in that coral explains their annual linear extension correlation to SST. The growth effect threshold for coral Ba/Ca has not been evaluated for any coral species to date; however, the study Reuer et al. (2003), who compare *S. siderea* and *M. annularis* offshore of Venezuela (Table 1), report no evidence for a growth effect in coral Ba/Ca. The lack of correlation between annual linear extension and coral Sr/Ca and Ba/Ca in 05WFGB3-1-A (Supplementary Table 4) suggests there is no growth-related effect in this study, thus our coral elemental ratios reflect environmental forcing.

The study of DeLong et al. (2016) found sampling artifacts for *S. siderea* in coral Sr/Ca when extracting coral micro-samples off the synapticulothecal wall and in the columella that results in a cold bias, or an increase in coral Sr/Ca. The four paths in 05WFGB3-1-A1 were micro-milled by four people with varying skill levels in coral micro-sampling, resulting in suboptimal sampling for two paths in the top 40 mm of the coral (2000–2005; Section 3.1). However, coral Ba/Ca does not exhibit the same suboptimal sampling artifact (Fig. 4), thus barium is likely deposited more homogeneously in the *S. siderea* skeleton along a growth interval than strontium. Similarly, coral $\delta^{18}O$ in *S. siderea* is not sensitive to sampling path location in the coral skeleton whereas coral $\delta^{13}C$ is generally not as reproducible (DeLong et al., 2016). Sampling path sensitivities for coral Sr/Ca are reported in other massive coral species (Alibert et al., 2003; DeLong et al., 2013; Giry et al., 2010; Smith et al., 2006) and for coral Ba/Ca (Alibert and Kinsley, 2008). Since there is more oxygen in the coral $CaCO_3$ skeleton, the result for $\delta^{18}O$ is logical; however, there is ~600 times less barium in the coral skeleton than strontium thus the result for barium is not easily explained and warrants further investigation.

4.3. Coral Sr/Ca to temperature calibration

The slope of the calibration equation (−0.042 mmol/mol/°C; Eq. (1)) is similar to the slopes reported for *S. siderea* (−0.041 to −0.047 mmol/mol/°C) sampled with monthly resolution (DeLong et al., 2011; DeLong et al., 2014; Kuffner et al., 2017) with the slope of −0.043 mmol/mol/°C assessed as the best-performing slope for 37 corals (DeLong et al., 2014; Flannery et al., 2017; Kuffner et al., 2017). It is promising to see that a *S. siderea* coral growing in deeper water (23.8 m) results in approximately the same slope as *S. siderea* colonies growing at depths less than 4.0 m (DeLong et al., 2011; Kuffner et al., 2017).

The intercept of the calibration equation (9.945 mmol/mol; Eq. (1)) is less than (10.063–10.25 mmol/mol) other *S. siderea* studies (DeLong et al., 2011; DeLong et al., 2014). This could be attributed to the difference between SST and reef temperature at 23.8 m depth, which is 0.8 °C colder on average than WFGB-SST (1986–2005) and has a reduced temperature range by 1.6 °C. In situ temperature is the preferred temperature source for calibrating coral geochemistry (Jones et al., 2009), and this study used in situ temperature as did the other *S. siderea* studies (DeLong et al., 2011; DeLong et al., 2014; Kuffner et al., 2017). Alternatively, differences in seawater Sr/Ca could cause intercept differences (Corrège, 2006), but little seawater data have been collected on coral reefs to properly understand the potential for Sr/Ca variability impact on calibration equations (de Villiers et al., 1994; Lebrato et al., 2020).

4.4. Oil drilling and coral Ba/Ca in the northern Gulf of Mexico

The greatest coral Ba/Ca values in our study occur in 1983–1985 (Fig. 7) including winter minima and summer maxima. Annual minima in coral Ba/Ca follows the trends in annual barite production in the US (Kelly and Matos, 2014) (Fig. 8) after expansion of oil drilling in late 1970s suggesting a contemporaneous relationship between oil drilling in the northern Gulf of Mexico and coral Ba/Ca from WFGB. Annual barite production and consumption leads annual coral Ba/Ca by approximately two to three years and barite production is significantly correlated with the lags (r = 0.52 for a 3-year lag; Supplementary Table 5) because barite stockpiles take time to be shipped to the offshore drilling platforms to be used as drilling mud and dissolving in seawater after being released into the marine sediments. The use of barite increases with oil production until 1983 when oil prices dropped and the coral Ba/Ca captures this peak and decline. The sharp decrease in annual coral Ba/Ca after 1983 could be due to the reduction of new offshore oil wells where barite is used. The increased range of the coral Ba/Ca annual cycles for

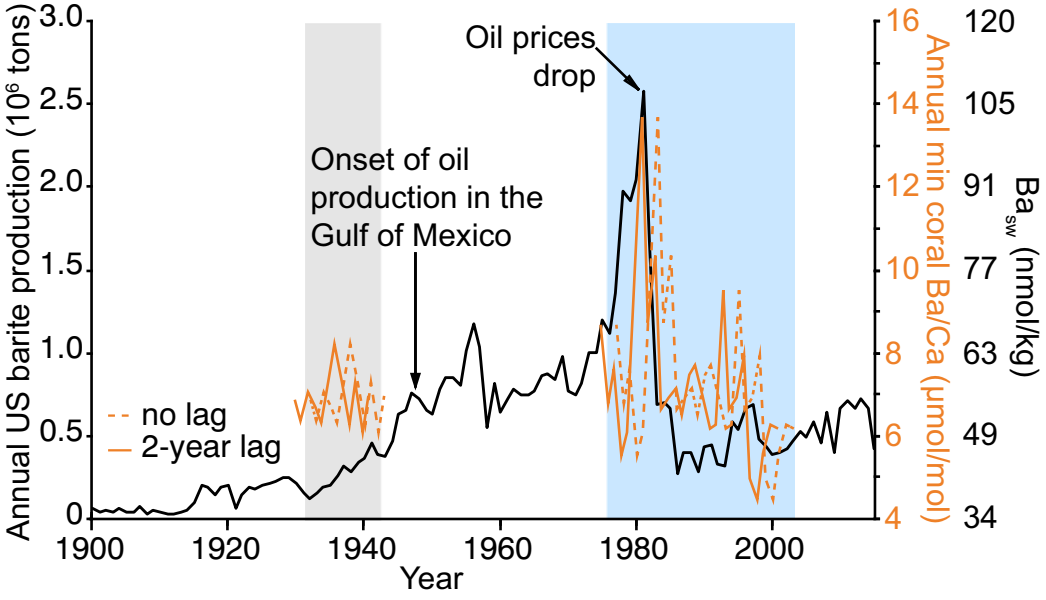

Fig. 8. Annual US barite production (black line) from 1900 to 2015 (Kelly and Matos, 2014) and annual minima coral Ba/Ca (orange dashed line) plotted with adjustment for two-year lag (solid orange line). Coral Ba/Ca is converted to seawater barium concentration (Ba_{sw}) using the *Porites* equation (LaVigne et al., 2016). The coral Ba/Ca in the blue area follows the annual US barite production with a 2 to 3 years lag whereas in the grey area it does not. (For interpretation of the references to colour in this figure legend, the reader is referred to the web version of this article.)

1976–2004 compared to the pre-oil industry interval 1931–1944 (Fig. 7) is the result of Ba enrichment in seawater increasing the monthly mean coral Ba/Ca and thus seasonal range.

The other coral Ba/Ca study in the Gulf of Mexico has a mean shift occurring ~1966 offshore of Veracruz Mexico (Carriquiry and Horta-Puga, 2010) when offshore oil exploration and drilling began in 1974 in the Campeche Sound (García-Cuéllar et al., 2004). Furthermore, that study noted the coral Ba/Ca lost correlation to the local river discharge signal after ~1975, suggesting the oil drilling barite signal overwhelmed the fluvial Ba signal. The other Ba/Ca studies in Caribbean (Table 1) do not have the mean shift seen in the Gulf of Mexico corals. Those sites are not near oil fields and they are upstream from WFGB in the prevailing currents, namely the Caribbean Current as it enters the Gulf of Mexico becoming the Loop Current (Fig. 1). Furthermore, the coral Ba/Ca values for other studies (Table 1) are generally less than those observed in the Gulf of Mexico regardless of coral species even those in upwelling zones. The exceptions are two sites with maximum coral Ba/Ca reaching 50 μmol/mol, Malindi Reef, Kenya (Fleitmann et al., 2007) where runoff dominates and New Ireland, Papua New Guinea (Alibert and Kinsley, 2008) where upwelling dominates; however, both of those studies used laser ablation ICP-MS with ~weekly resolution whereas the Gulf of Mexico studies use annual or monthly resolution that may not capture daily to weekly events.

The estimated increase in mean Ba concentration in seawater from 1931–1944 to 1976–2004 using the LaVigne et al. (2016) calibration for *Porites lobata* is ~13 nmol/kg (Fig. 8); however, this calibration is species-specific and may differ for *S. siderea*. The equation for *P. lobata* was used because it provided the most conservative Ba seawater estimate. Dissolved Ba concentration in the Gulf of Mexico is ~73 nmol/kg in open water to ~357 nmol/kg in coastal Louisiana (Boothe and Presley, 1987; Chan and Hanor, 1982). The saturation of barite in seawater occurs at approximately ~150 nmol/kg (Church and Wolgemuth, 1972) and thus it is commonly undersaturated in the Gulf of Mexico (Deslarzes et al., 1995) as in the rest of the ocean (Carter et al., 2020). However, the study of Chan and Hanor (1982) found Ba concentrations above the level of saturation in the northern Gulf of Mexico in the late 1970s, when the US barite production and consumption escalated (Fig. 8), thus provides evidence of increased Ba in the seawater during times of increased offshore oil drilling operations. The previously estimated increase in seawater Ba concentration due to barite dissolution by Deslarzes et al. (1995) was ~109 nmol/kg, which is much higher than our increase estimate. That study assumed dissolved Ba does not transport away from the drilling area; therefore, their higher estimation may not be realistic. Some early studies found seawater barium concentration decreases with time and distance from a drill site because most of the drilling muds released onto the seafloor are transported away by currents (Boothe and Presley, 1987). The amount of Ba retained in the sediment near a drill site after one year is ~1% of the total Ba used in drilling (Boothe and Presley, 1987). Additionally, surface seawater Ba concentration is further reduced through primary production where barite attaches to sinking organic matter further reducing the surface Ba seawater concentration with time. In order to better estimate the historical changes in seawater Ba in the Gulf of Mexico, a species-specific Ba seawater calibration is needed along with seawater barium measurements spanning at least one year, similar to the study of LaVigne et al. (2016).

Oil drilling operations use barite ($BaSO_4$) as a densifying material in the drilling mud and accounts for 90% of the US barite consumption (Crecelius et al., 2007). Barite contains trace metals such as mercury (Hg) and cadmium (Cd) as impurities. The US Environment Protection Agency has imposed regulations for discharging barite in drilling fluids into the Gulf of Mexico such that the maximum concentrations should be below 1 μg/g for Hg and 3 μg/g for Cd, which are found in barite used in oil drilling mud (Crecelius et al., 2007). Barite is insoluble in normal seawater pH (7.9–8.1) and oxidizing conditions; however, the solubility increases with more acidic pH and in anoxic-reducing environments (Carbonell et al., 1999; Crecelius et al., 2007). The study of Trefry et al. (2007) revealed elevated total Hg levels in sediments near six drilling sites in the Gulf of Mexico east of WFGB that were associated with barite from drilling mud. They found less methyl-Hg due to the formation of insoluble metal sulfides indicating anoxic, highly reducing conditions in sediments near drill sites. Therefore, the presence of anoxic conditions at drill sites could be favorable to dissolving Ba from barite at offshore oil drilling sites. Mid-summer hypoxia in the northern Gulf of Mexico occurs because of enhanced surface production forming excess organic matter that sinks to the bottom and decay, causing hypoxia below the pycnocline (Rabalais et al., 2002), which could also promote barite to dissolve. Bottom water hypoxia can persist throughout the year due to the stability of the density difference between surface and bottom water (Rabalais et al., 1991; Wiseman et al., 1997). Benthic organisms are vulnerable to ingesting barite that can dissolve inside their gut (acidic) and release heavy metals such as Hg, Cd, Zn, and Cu (Crecelius et al., 2007). The bioavailability of these metals can lead to bioaccumulation along food chains and cause health risks to local fish consumers as well.

4.5. Coral Ba/Ca in S. siderea

The study of LaVigne et al. (2016) examined coral Ba/Ca in multiple Pacific coral taxa in the Gulf of Panama and found inconsistencies in distribution coefficients, linear regression slopes, and intercepts that provided robust evidence for a species effect in coral Ba/Ca. The mean coral Ba/Ca measured in *S. siderea* from WFGB is ~50% greater than the means reported for *Montastraea* corals (~8.0 μmol/mol) in the Gulf of Mexico (Table 1) (Carriquiry and Horta-Puga, 2010; Deslarzes et al., 1995) with a maximum value of 28.52 μmol/mol (Table 2), which is 280% greater than those previous studies. The *M. annularis* sampled in the study of Deslarzes et al. (1995) and the *S. siderea* sampled in this study are from the same reef and water depth providing evidence for a species effect for coral Ba/Ca at WFGB. A study in the southern Caribbean Sea also found greater coral Ba/Ca values in *S. siderea* when compared with co-located *M. annularis* (Reuer et al., 2003). Similar species effects have been reported for coral Sr/Ca and $\delta^{18}O$ (Bagnato et al., 2005; Dassié and Linsley, 2015; DeLong et al., 2011; Ross et al., 2019; Weber, 1973). Regardless of the species differences in coral Ba/Ca, this study and the study of Carriquiry and Horta-Puga (2010) document a mean shift in coral Ba/Ca of 1.76 and 1.03 μmol/mol, respectively, for the interval before and during oil exploration in the Gulf.

Coral Ba/Ca annual cycles are ~180° out of phase with coral Sr/Ca annual cycles and differ (Fig. 7), thus indicating the coral Ba/Ca annual cycles are driven by a different seasonally-varying environmental factor than temperature. Possible factors driving variations in coral Ba/Ca include (1) river discharge, (2) extreme events such as hurricanes, (3) upwelling driven by winds, and (4) sea surface productivity, thus we will investigate each of these further.

The Mississippi, Atchafalaya, Trinity, and Rio Grande Rivers are the main rivers bringing water and sediments into the northwestern Gulf of Mexico (Fig. 1). Barium is desorbed from sediment particles and dissolves in seawater increasing Ba concentrations in the river mixing zones and coastal waters (Bishop, 1988; Ganeshram et al., 2003). The Mississippi River discharge (average 16,792 m^3/s) varies seasonally with a maximum in April due to snowmelt and spring floods in the US with a minimum in August to September (Fig. 7) (Wagner and Slowey, 2011). Wind-driven coastal currents over the continental shelf in the northern Gulf of Mexico flow eastward in summer and westward in winter along the coastline (Fig. 1) (Walker, 2005). Mississippi River plumes are carried westward during the winter through a low salinity band that is confined to the coastline by onshore Ekman transport (Schiller et al., 2011). When the wind reversal brings westerly winds in March and April, the low salinity band broadens offshore but the river plume is transported towards the east from the Mississippi River delta (Schiller et al., 2011). The average discharge of Atchafalaya (6185.5 m^3/s),

Trinity (177.5 m^3/s and closest river to WFGB), and Rio Grande (82 m^3/s) Rivers is much lower than the Mississippi River and their waters are also distributed from the north to the south along the Texas coast away from WFGB. Salinity measurements in the summer do not indicate freshening at WFGB (Li et al., 1997; Wagner and Slowey, 2011; Johnston et al., 2020). The variability of seawater $\delta^{18}O$ (1.0‰–1.2‰) and salinity (35.7–36.6) has a narrow range throughout the year at WFGB when compared with the inner shelf waters (Wagner and Slowey, 2011) suggesting Mississippi River waters are not reaching WFGB with seasonal regularity. Furthermore, the coral Ba/Ca maxima are not synchronous with major Mississippi River flood events (April 1979, May 1983, March 1997, and April 2002; Fig. 7) (National Weather Service, 2019). Therefore, river plumes are kept away from the WFGB throughout the year, thus the probability of river discharge manifesting as regular coral Ba/Ca annual cycles is not likely. A study of the inner shelf and outer shelf corals in the Great Barrier Reef (Walther et al., 2013) found the inner shelf coral Ba/Ca variability was driven by river runoff whereas the outer shelf (~100 km away from the coast) coral Ba/Ca variability was dominated by seasonal and interannual oceanographic variability such as upwelling. Another Great Barrier Reef study measured coral Ba/Ca from the river mixing zones along the coast (~200 km) and they found coral Ba/Ca is driven by river discharge only in corals in close proximity to river mouths (Lewis et al., 2018). If Mississippi River waters were regularly reaching WFGB, these coral reefs would probably not exist since corals need clear water for photosynthesis (Veron, 1995). Flower Garden Banks' coral reefs are in a special place, on rising salt domes at the edge of the continental shelf far from land, thus why they are the only coral reefs in the northern Gulf of Mexico. This holds true for submerged fossil reefs in the Gulf, they are all far from the Mississippi River, such as the southern Texas Coast (Khanna et al., 2017).

Hurricanes can produce vertical mixing and rapid ventilation of the thermocline due to high wind speeds that mix nutrient-rich colder waters to the surface (Walker et al., 2005). These events are short-lived but can produce phytoplankton blooms that peak three to four days after a tropical cyclone passes (Walker et al., 2005). There have been four category one hurricanes (wind speed 119–153 km/h): Alicia August 17, 1983, Bonnie June 26, 1986, Chantal August 1, 1989, and Jerry October 15, 1989, passing over and near WFGB from 1976 to 2004 (Landsea and Franklin, 2013) that could bring barium-enriched colder water to the surface. The coral Ba/Ca record does not reveal anomalously high peak values that coincide with the timing of any of these four hurricanes (Fig. 7). These extreme events are short-lived (a few days) and they do not occur with enough regularity to explain the coral Ba/Ca annual cycles. Lastly, a monthly-resolved coral geochemical record would not record an event that spans a few days (Kilbourne et al., 2010).

Reef temperature measured instrumentally at WFGB (Johnston et al., 2020) and reconstructed via coral Sr/Ca (Fig. 4) do not provide evidence for cold-water upwelling. The *S. siderea* coral sampled in this study is located at a depth of 23.8 m at the edge of the continental shelf that slopes down to deeper waters (Fig. 1). The continental shelf edge could experience weak springtime upwelling when the winds reverse in March and April (Murray et al., 1998; Teague et al., 2013), thus explaining the small springtime (March–April) coral Ba/Ca increase that is prominent in both time intervals but this does not explain the subsequent summer increase of coral Ba/Ca (Fig. 7).

The biogeochemical cycle of barium in seawater reflects surface oceanic depletion of barium that is recycled at depth resulting in a nutrient-like depth profile (Carter et al., 2020; Chow and Goldberg, 1960). The removal of Ba at the ocean surface is associated with the precipitation of Ba as $BaSO_4$ (barite) crystals, especially in micro-environments such as decaying organic matter (Chow and Goldberg, 1960) at times of enhanced surface productivity. Sinking organic matter from the surface recycles below the thermocline where $BaSO_4$ crystals dissolve to make Ba available at depth (Chan et al., 1977). This mechanism explains the relationship between Ba depletion and biological productivity at the ocean surface, and the annual cycles in coral Ba/Ca, although Ba is not actively involved in productivity.

Satellite-derived estimates of chlorophyll-a every eight days from the Sea Viewing Wide Field of View Sensor (SeaWiFS) are a productivity indicator that is limited temporally (1997–2010; Fig. 9). The SeaWiFS chlorophyll-a data was linearly interpolated to monthly intervals for correlation with monthly-resolved coral Ba/Ca ($r = -0.50$; $n = 76$; Fig. 9). Winter months have a higher chlorophyll-a concentration in the Gulf of Mexico due to increased depth of the mixed layer by wind-driven mixing (Müller-Karger et al., 1991) that corresponds with the coral Ba/Ca minima thus increase in chlorophyll-a concentration and productivity drive the coral Ba/Ca to lower values and when productivity decreases in the summer the coral Ba/Ca increases (Fig. 9). The regular seasonal changes in surface productivity at WFGB explains 25% of the variance in the monthly coral Ba/Ca for 1997.5–2003.96. Time assignment with coral Sr/Ca to WFGB-SST may result in minor month-to-month dating discrepancies (±2–3 months) that are difficult to resolve (DeLong et al., 2016) but may partially explain the lower than expected correlation between monthly coral Ba/Ca and chlorophyll-a yet the monthly coral Ba/Ca does capture some of the chlorophyll-a 8-day variability (Fig. 9). Micro-sampling the coral at weekly resolution may provide better results with chlorophyll-a but would still be subject to subannual dating uncertainties. Regardless, the connection between

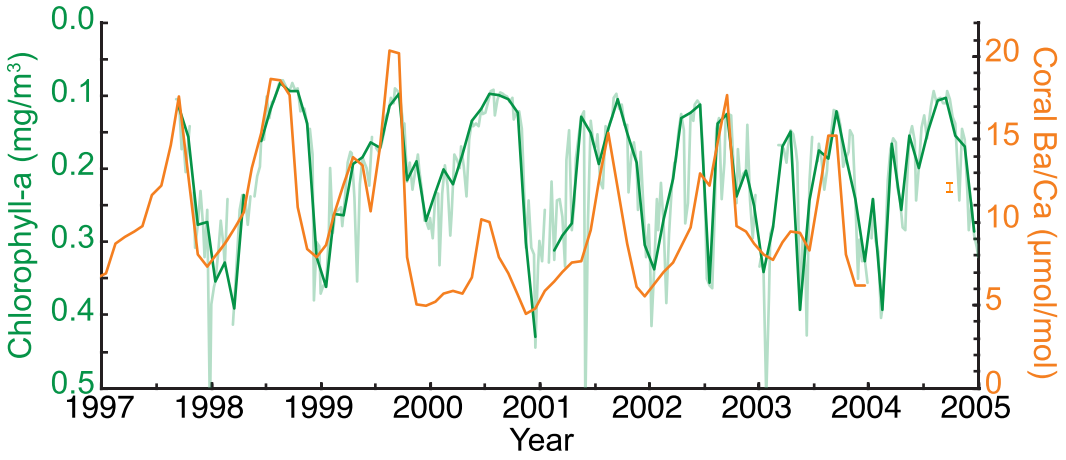

Fig. 9. Monthly-resolved coral Ba/Ca and eight-day chlorophyll-a concentration for WFGB area linearly resampled to monthly intervals (light green and green, respectively). Error bar is analytical precision (2σ). Satellite-derived chlorophyll-a is plotted inversed from SeaWiFS for the area 27.4°N to 28.1°N and 94°W to 93.25°W (https://oceancolor.gsfc.nasa.gov/SeaWiFS/). (For interpretation of the references to colour in this figure legend, the reader is referred to the web version of this article.)

coral Ba/Ca and ocean surface productivity should be explored further and WFGB is an ideal location for such a study since it is located far from the coast, river discharge, and is submerged with minimal upwelling occurring.

5. Conclusions

Coral Ba/Ca is a complex proxy that is affected by multiple environmental factors, depending on the location and time scale of measurement. *S. siderea* incorporates more Ba into its coral skeleton than other coral species in the Gulf of Mexico and exhibits distinct annual coral Ba/Ca cycles likely driven by interactions of productivity and spring-time upwelling. Interannual variability and long-term mean changes in coral Ba/Ca appear to be associated with barite used in offshore oil drilling in the northern Gulf of Mexico. Barite ingestion by benthic organisms may enhance bioavailability of heavy metals such as Hg and Cd that can lead to potential biomagnification towards the high end of the food chains. Coral Ba/Ca can be used as a tracer to determine marine environment pollution associated with oil drilling in the Gulf of Mexico.

CRediT authorship contribution statement

Mudith M. Weerabaddana: Investigation, Methodology, Formal analysis, Writing – original draft, Visualization, Data curation, Validation. **Kristine L. DeLong:** Conceptualization, Funding acquisition, Formal analysis, Investigation, Methodology, Project administration, Resources, Supervision, Validation, Data curation, Writing – review & editing. **Amy J. Wagner:** Conceptualization, Funding acquisition, Investigation, Resources, Writing – review & editing. **Deborah W.Y. Loke:** Conceptualization, Methodology, Investigation. **K. Halimeda Kilbourne:** Resources, Validation, Writing – review & editing. **Niall Slowey:** Conceptualization, Funding acquisition, Resources. **Hsun-Ming Hu:** Resources, Validation. **Chuan-Chou Shen:** Resources, Validation, Writing – review & editing.

Declaration of competing interest

The authors declare that they have no known competing financial interests or personal relationships that could have appeared to influence the work reported in this paper.

Acknowledgements

We would like to thank our funding sources, the Department of the Interior South Central Climate Adaptation Science Center Cooperative Agreement G15AP00136 for supporting this research, the European Union Erasmus+ scholarship (to M.M.W), and the Haus der Kulturen der Welt - Earth Indices, Evidence, and Experiment project, part of the Anthropocene Curriculum (to K.L.D). ^{230}Th dating and trace elemental analysis in the HISPEC Laboraory was supported by grants from the Science Vanguard Research Program of the Ministry of Science and Technology (MOST) (108-2119-M-002-012, 109-2123-M-002-001 to C.-C.S.), the National Taiwan University (109L8926 to C.-C.S.), the Higher Education Sprout Project of the Ministry of Education, Taiwan ROC (109L901001 to C.-C.S.). This work represents UMCES contribution #6047 for K.H.K. We are deeply grateful to the Flower Garden Banks National Marine Sanctuary for their assistance and access to corals and data resources. Corals were collected under permit FGBNMS-2005-002. Ginesse Listi and Mary Manheim of the LSU FACES Laboratory are thanked for their assistance with the coral X-radiographs. Fred Taylor and Jud Partin at the University of Texas Institute for Geophysics for assisting with core slabbing. We thank LSU PAST Laboratory students Jacob Warner, Elizabeth Cruzado Carranza, Jessica Tolen, Othalia Roberts, and Kendall Brome for their support during this project as well as Michelle LaVigne for her insights into coral Ba/Ca. We thank the anonymous reviewers and editors for their suggestions to improve this report. Coral data associated with this article are archived at the National Centers for Environmental Information-Paleoclimatology, 325 Broadway, Boulder, Colorado; IGBP PAGES/World Data Center for Paleoclimatology https://www.ncdc.noaa.gov/paleo-search/study/34032.

Appendix A. Supplementary data

Supplementary data to this article can be found online at https://doi.org/10.1016/j.marpolbul.2021.112930.

References

Alibert, C., Kinsley, L., 2008. A 170-year Sr/Ca and Ba/Ca coral record from the western Pacific warm pool: 1. What can we learn from an unusual coral record? J. Geophys. Res. Oceans 113 (C4), C04008. https://doi.org/10.1029/2006JC003979.

Alibert, C., Kinsley, L., Fallon, S.J., McCulloch, M.T., Berkelmans, R., McAllister, F., 2003. Source of trace element variability in Great Barrier Reef corals affected by the Burdekin flood plumes. Geochim. Cosmochim. Acta 67 (2), 231–246.

Alibert, C., McCulloch, M.T., 1997. Strontium/calcium ratios in modern *Porites* corals from the Great Barrier Reef as a proxy for sea surface temperature: calibration of the thermometer and monitoring of ENSO. Paleoceanography 12 (3), 345–363. https://doi.org/10.1029/97PA00318.

Bagnato, S., Linsley, B.K., Howe, S.S., Wellington, G.M., Salinger, J., 2005. Coral oxygen isotope records of interdecadal climate variations in the South Pacific Convergence Zone region. Geochem. Geophys. Geosyst. 6 (6), Q06001 https://doi.org/10.1029/2004GC000879.

Bishop, J.K., 1988. The barite-opal-organic carbon association in oceanic particulate matter. Nature 332 (6162), 341–343. https://doi.org/10.1038/332341a0.

Boothe, P.N., Presley, B.J., 1987. The effects of exploratory petroleum drilling in the northwest Gulf of Mexico on trace metal concentrations in near rig sediments and organisms. Environ. Geol. Water Sci. 9 (3), 173–182.

Bryan, S.P., Hughen, K.A., Karnauskas, K.B., Farrar, J.T., 2019. Two hundred fifty years of reconstructed South Asian summer monsoon intensity and decadal-scale variability. Geophys. Res. Lett. 46 (7), 3927–3935. https://doi.org/10.1029/2018gl081593.

Buddemeier, R.W., Maragos, J.E., 1974. Radiographic studies of reef coral exoskeletons: rates and patterns of coral growth. J. Exp. Mar. Biol. Ecol. 14, 179–200.

Cantarero, S.I., Tanzil, J.T.I., Goodkin, N.F., 2017. Simultaneous analysis of Ba and Sr to Ca ratios in scleractinian corals by inductively coupled plasma optical emissions spectrometry. Lim. Ocean. Met. 15 (1), 116–123. https://doi.org/10.1002/lom3.10152.

Carbonell, A.A., Pulido, R., DeLaune, R.D., Patrick Jr., W.H., 1999. Soluble barium in barite and phosphogypsum amended Mississippi River alluvial sediment. J. Environ. Qual. 28 (1), 316–321. https://doi.org/10.2134/jeq1999.00472425002800010039x.

Carilli, J.E., Prouty, N.G., Hughen, K.A., Norris, R.D., 2009. Century-scale records of land-based activities recorded in Mesoamerican coral cores. Mar. Pollut. Bull. 58 (12), 1835–1842. https://doi.org/10.1016/j.marpolbul.2009.07.024.

Carriquiry, J.D., Horta-Puga, G., 2010. The Ba/Ca record of corals from the southern Gulf of Mexico: Contributions from land-use changes, fluvial discharge and oil-drilling muds. Mar. Pollut. Bull. 60 (9), 1625–1630. https://doi.org/10.1016/j.marpolbul.2010.06.007.

Carter, S.C., Paytan, A., Griffith, E.M., 2020. Toward an improved understanding of the marine barium cycle and the application of marine barite as a paleoproductivity proxy. Minerals 10 (5), 421. https://doi.org/10.3390/min10050421.

Chan, L.-H., Hanor, J.S., 1982. Dissolved barium in some Louisiana offshore waters: problems in establishing baseline values. Contrib. Mar. Sci. 25, 149–159.

Chan, L.H., Drummond, D., Edmond, J.M., Grant, B., 1977. On the barium data from the Atlantic GEOSECS expedition. Deep-Sea Res. 24 (7), 613–649. https://doi.org/10.1016/0146-6291(77)90505-7.

Chen, T., Yu, K., Li, S., Chen, T., Shi, Q., 2011. Anomalous Ba/Ca signals associated with low temperature stresses in *Porites* corals from Daya Bay, northern South China Sea. J. Environ. Sci. 23 (9), 1452–1459. https://doi.org/10.1016/S1001-0742(10)60606-7.

Chen, X., Deng, W., Wei, G., McCulloch, M., 2020. Terrestrial signature in coral Ba/Ca, δ^{18}O, and δ^{13}C records from a macrotide-dominated nearshore reef environment, Kimberley region of northwestern Australia. J. Geophys. Res. Biogeosci. 125 (3), e2019JG005394 https://doi.org/10.1029/2019jg005394.

Cheng, H., Edwards, R.L., Shen, C.-C, Polyak, V.J., Asmerom, Y., Woodhead, J., Hellstrom, J., Wang, Y., Kong, X., Spötl, C., Wang, X., Alexander Jr., C., 2013. Improvements in ^{230}Th dating, ^{230}Th and ^{234}U half-life values, and U-Th isotopic measurements by multi-collector inductively coupled plasma mass spectrometry. Earth Planet. Sci. Lett. 371, 82–91. https://doi.org/10.1016/j.epsl.2013.04.006.

Chow, T.J., Goldberg, E.D., 1960. On the marine geochemistry of barium. Geochim. Cosmochim. Acta 20 (3), 192–198. https://doi.org/10.1016/0016-7037(60)90073-9.

Church, T.M., Wolgemuth, K., 1972. Marine barite saturation. Earth Planet. Sci. Lett. 15 (1), 35–44. https://doi.org/10.1016/0012-821X(72)90026-X.

Corrège, T., 2006. Sea surface temperature and salinity reconstruction from coral geochemical tracers. Palaeogeogr. Palaeoclimatol. Palaeoecol. 232 (2–4), 408–428. https://doi.org/10.1016/j.palaeo.2005.10.014.

Crecelius, E., Trefry, J., McKinley, J., Lasorsa, B., Trocine, R., 2007. Study of barite solubility and the release of trace components to the marine environment, Final Report. In: U.S. Department of the Interior, Minerals Management Services, Gulf of Mexico OCS Region, OCS Study 2007-061. Obligation No.: 1435-01-02-RP-70000 (M03PC00001). OCS Study MMS, New Orleans, LA. https://marinecadastre.gov/espis/#/search/study/213.

Darnell, R.M., Defenbaugh, R.E., 1990. Gulf of Mexico: Environmental overview and history of environmental research. Am. Zool. 30 (1), 3–6. https://doi.org/10.1093/icb/30.1.3.

Dassié, E.P., Linsley, B.K., 2015. Refining the sampling approach for the massive coral *Diploastrea heliopora* for $\delta^{18}O$-based paleoclimate applications. Palaeogeogr. Palaeoclimatol. Palaeoecol. 440, 274–282. https://doi.org/10.1016/j.palaeo.2015.08.043.

de Villiers, S., Greaves, M., Elderfield, H., 2002. An intensity ratio calibration method for the accurate determination of Mg/Ca and Sr/Ca of marine carbonates by ICP-AES. Geochem. Geophys. Geosyst. 3 (1) https://doi.org/10.1029/2001GC000169.

de Villiers, S., Shen, G.T., Nelson, B.K., 1994. The Sr/Ca-temperature relationship in coralline aragonite: Influence of variability in $(SrCa)_{seawater}$ and skeletal growth parameters. Geochim. Cosmochim. Acta 58 (1), 197–208. https://doi.org/10.1016/0016-7037(94)90457-x.

DeLong, K.L., Flannery, J.A., Maupin, C.R., Poore, R.Z., Quinn, T.M., 2011. A coral Sr/Ca calibration and replication study of two massive corals from the Gulf of Mexico. Palaeogeogr. Palaeoclimatol. Palaeoecol. 307 (1–4), 117–128. https://doi.org/10.1016/j.palaeo.2011.05.005.

DeLong, K.L., Flannery, J.A., Poore, R.Z., Quinn, T.M., Maupin, C.R., Lin, K., Shen, C.-C, 2014. A reconstruction of sea surface temperature variability in the southeastern Gulf of Mexico from 1734 to 2008 C.E. using cross-dated Sr/Ca records from the coral *Siderastrea siderea*. Paleoceanography 29 (5), 403–422. https://doi.org/10.1002/2013PA002524.

DeLong, K.L., Maupin, C.R., Flannery, J.A., Quinn, T.M., Shen, C.-C., 2016. Refining temperature reconstructions with the Atlantic coral *Siderastrea siderea*. Palaeogeogr. Palaeoclimatol. Palaeoecol. 462, 1–15. https://doi.org/10.1016/j.palaeo.2016.08.028.

DeLong, K.L., Quinn, T.M., Taylor, F.W., 2007. Reconstructing twentieth-century sea surface temperature variability in the southwest Pacific: a replication study using multiple coral Sr/Ca records from New Caledonia. Paleoceanography 22 (4), PA4212. https://doi.org/10.1029/2007PA001444.

DeLong, K.L., Quinn, T.M., Taylor, F.W., Shen, C.-C., Lin, K., 2013. Improving coral-base paleoclimate reconstructions by replicating 350 years of coral Sr/Ca variations. Palaeogeogr. Palaeoclimatol. Palaeoecol. 373, 6–24. https://doi.org/10.1016/j.palaeo.2012.08.019.

Deslarzes, K.J.P., 1992. In: Long-term monitoring of reef corals at Flower Garden Banks (northwest Gulf of Mexico): Reef coral populations changes and historical incorporation of barium in *Montastrea annularis*. Texas A&M University, College Station.

Deslarzes, K.J.P., Boothe, P.N., Presley, B.J., Steinmetz, G.L., 1995. Historical incorporation of barium in the reef building coral *Montastrea annularis* at the Flower Garden Banks, north-west Gulf of Mexico. Mar. Pollut. Bull. 30, 718–722.

Edmond, J.M., Boyle, E.D., Drummond, D., Grant, B., Mislick, T., 1978. Desorption of barium in the plume of the Zaire (Congo) river. Neth. J. Sea Res. 12 (3), 324–328. https://doi.org/10.1016/0077-7579(78)90034-0.

Fallon, S.J., McCulloch, M.T., van Woesik, R., Sinclair, D.J., 1999. Corals at their latitudinal limits: laser ablation trace element systematics in *Porites* from Shirigai Bay, Japan. Earth Planet. Sci. Lett. 172 (3–4), 221–238. https://doi.org/10.1016/S0012-821X(99)00200-9.

Flannery, J.A., Richey, J.N., Thirumalai, K., Poore, R.Z., DeLong, K.L., 2017. Multi-species coral Sr/Ca-based sea-surface temperature reconstruction using *Orbicella Faveolata* and *Siderastrea siderea* from the Florida Straits. Palaeogeogr. Palaeoclimatol. Palaeoecol. 466, 100–109. https://doi.org/10.1016/j.palaeo.2016.10.022.

Fleitmann, D., Dunbar, R.B., McCulloch, M., Mudelsee, M., Vuille, M., McClanahan, T.R., Cole, J.E., Eggins, S., 2007. East African soil erosion recorded in a 300 year old coral colony from Kenya. Geophys. Res. Lett. 34 (4), L04401 https://doi.org/10.1029/2006GL028525.

Ganeshram, R.S., François, R., Commeau, J., Brown-Leger, S.L., 2003. An experimental investigation of barite formation in seawater. Geochim. Cosmochim. Acta 67 (14), 2599–2605. https://doi.org/10.1016/S0016-7037(03)00164-9.

García-Cuéllar, J.A., Arreguín-Sánchez, F., Vázquez, S.H., Lluch-Cota, D.B., 2004. Ecological impact of the oil industry on the Campeche Sound, Mexico, after three decades of activities: A review. Interciencia 29 (6), 311–319.

Giry, C., Felis, T., Kölling, M., Scheffers, S., 2010. Geochemistry and skeletal structure of *Diploria strigosa*, implications for coral-based climate reconstruction. Palaeogeogr. Palaeoclimatol. Palaeoecol. 298 (3–4), 378–387. https://doi.org/10.1016/j.palaeo.2010.10.022.

Goodkin, N.F., Hughen, K.A., Cohen, A.L., 2007. A multicoral calibration method to approximate a universal equation relating Sr/Ca and growth rate to sea surface temperature. Paleoceanography 22 (1), PA1214. https://doi.org/10.1029/2006PA001312.

Grove, C.A., Zinke, J., Peeters, F., Park, W., Scheufen, T., Kasper, S., Randriamanantsoa, B., McCulloch, M.T., Brummer, G.-J.A., 2013. Madagascar corals reveal a multidecadal signature of rainfall and river runoff since 1708. Clim. Past 9 (2), 641–656. https://doi.org/10.5194/cp-9-641-2013.

Grove, C.A., Zinke, J., Scheufen, T., Maina, J., Epping, E., Boer, W., Randriamanantsoa, B., Brummer, G.-J.A., 2012. Spatial linkages between coral proxies of terrestrial runoff across a large embayment in Madagascar. Biogeosciences 9 (8), 3063–3081. https://doi.org/10.5194/bg-9-3063-2012.

Guzmán, H.M., Tudhope, A.W., 1998. Seasonal variation in skeletal extension rate and stable isotopic ($^{13}C/^{12}C$ and $^{18}O/^{16}O$) composition in response to several environmental variables in the Caribbean reef coral *Siderastrea siderea*. Mar. Ecol. Prog. Ser. 166, 109–118. https://doi.org/10.3354/meps166109.

Hart, S.R., Cohen, A.L., 1996. An ion probe study of annual cycles of Sr/Ca and other trace elements in corals. Geochim. Cosmochim. Acta 60, 3075–3084. https://doi.org/10.1016/0016-7037(96)00154-8.

Hathorne, E.C., Gagnon, A., Felis, T., Adkins, J., Asami, R., Boer, W., Caillon, N., Case, D., Cobb, K.M., Douville, E., deMenocal, P., Eisenhauer, A., Schönberg, D.G-., Geibert, W., Goldstein, S., Hughen, K., Inoue, M., Kawahata, H., Kölling, M., Cornec, F.L., Linsley, B.K, McGregor, H.V., Montagna, P., Nurhati, I.S., Quinn, T.M, Raddatz, J., Rebaubier, H., Robinson, L., Sadekov, A., Sherrell, R., Sinclair, D., Tudhope, A.W., Wei, G., Wong, H., Wu, H.C., You, C.-F., 2013. Interlaboratory study for coral Sr/Ca and other element/Ca ratio measurements. Geochem. Geophys. Geosyst. 14 (9), 3730–3750. https://doi.org/10.1002/ggge.20230.

Horta-Puga, G., Carriquiry, J.D., 2012. Coral Ba/Ca molar ratios as a proxy of precipitation in the northern Yucatan Peninsula, Mexico. Appl. Geochemistry 27 (8), 1579–1586. https://doi.org/10.1016/j.apgeochem.2012.05.008.

Ito, S., Watanabe, T., Yano, M., Watanabe, T.K., 2020. Influence of local industrial changes on reef coral calcification. Sci. Rep. 10 (1), 1–11. https://doi.org/10.1038/s41598-020-64877-6.

Jiang, Q., Cao, Z., Wang, D., Li, Y., Wu, Z., Ni, J., 2017. Coral Ba/Ca and Mn/Ca ratios as proxies of precipitation and terrestrial input at the eastern offshore area of Hainan Island. J. Ocean Univ. China 16 (6), 1072–1080. https://doi.org/10.1007/s11802-017-3265-0.

Johnston, M.A., Blakeway, R.D., O'Connell, K, MacMillan, J., Nuttall, M.F., Hu, X, Embesi, J.A., Hickerson, E.L., Schmahl, G.P., 2020. Long-term monitoring at East and West Flower Garden Banks: 2018 annual report. Department of Commerce, National Oceanic and Atmospheric Administration, Flower Garden Banks National Marine Sanctuary, Galveston, TX. https://sanctuaries.noaa.gov/science/conservation/fgbnms-long-term-monitoring-report.html.

Jones, P.D., Briffa, K.R., Osborn, T.J., Laugh, J.M., van Ommen, T.D., Vinther, B.M., Luterbacher, J., Wahl, E.R., Zwiers, F.W., Mann, M.E., Schmidt, G.A., Ammann, C. M., Buckley, B.M., Cobb, K.M., Espre, J., Goosse, H., Graham, N., Jansen, E., Kaifer, T., Kull, C., Küttel, M., Mosley-Thompson, E., Overpeck, J.T., Riedwyl, N., Schulz, M., Tudhope, A.W., Villalba, R., Wanner, H., Wolff, E., Xoplaki, E., 2009. High-resolution palaeoclimatology of the last millennium: a review of current status and future prospects. Holocene 19 (1), 3–49. https://doi.org/10.1177/0959683608098952.

Jupiter, S., Roff, G., Marion, G., Henderson, M., Schrameyer, V., McCulloch, M., Hoegh-Guldberg, O., 2008. Linkages between coral assemblages and coral proxies of terrestrial exposure along a cross-shelf gradient on the southern Great Barrier Reef. Coral Reefs 27 (4), 887–903. https://doi.org/10.1007/s00338-008-0422-3.

Kasper-Zubillaga, J.J., Armstrong-Altrin, J.S., Rosales-Hoz, L., 2014. Geochemical study of coral skeletons from the Puerto Morelos Reef, southeastern Mexico. Estuar. Coast. Shelf Sci. 151, 78–87. https://doi.org/10.1016/j.ecss.2014.09.023.

Kelly, T.D., Matos, G.R., comps., 2014. Historical statistics for mineral and material commodities in the United States (2016 version), U.S. Geological Survey Data Series 140, https://www.usgs.gov/centers/nmic/historical-statistics-mineral-and-material-commodities-united-states.

Khanna, P., Droxler, A.W., Nittrouer, J.A., Tunnell Jr., J.W., Shirley, T.C., 2017. Coralgal reef morphology records punctuated sea-level rise during the last deglaciation. Nat. Commun. 8, 1046. https://doi.org/10.1038/s41467-017-00966-x.

Kilbourne, K.H., Quinn, T.M., Webb, R., Guilderson, T., Nyberg, J., Winter, A., 2010. Coral windows onto seasonal climate variability in the northern Caribbean since 1479. Geochem. Geophys. Geosyst. 11, Q10006. https://doi.org/10.1029/2010gc003171.

Knutson, D.W., Buddemeier, R.W., Smith, S.V., 1972. Coral chronometers: seasonal growth bands in reef corals. Science 177 (4045), 270–272. https://doi.org/10.1126/science/177.4045.270.

Kuffner, I.B., Roberts, K.E., Flannery, J.A., Morrison, J.M., Richey, J.N., 2017. Fidelity of the Sr/Ca proxy in recording ocean temperature in the western Atlantic coral *Siderastrea siderea*. Geochem. Geophys. Geosyst. 18 (1), 178–188. https://doi.org/10.1002/2016GC006640.

Landsea, C.W., Franklin, J.L., 2013. Atlantic hurricane database uncertainty and presentation of a new database format. Mon. Weather Rev. 141 (10), 3576–3592. https://doi.org/10.1175/mwr-d-12-00254.1.

LaVigne, M., Grottoli, A.G., Palardy, J.E., Sherrell, R.M., 2016. Multi-colony calibrations of coral Ba/Ca with a contemporaneous in situ seawater barium record. Geochim. Cosmochim. Acta 179, 203–216. https://doi.org/10.1016/j.gca.2015.12.038.

Lea, D.W., Shen, G.T., Boyle, E.A., 1989. Coralline barium records temporal variability in equatorial Pacific upwelling. Nature 340 (6232), 373–376. https://doi.org/10.1038/340373a0.

Lebrato, M., Garbe-Schönberg, D., Müller, M.N., Blanco-Ameijeiras, S., Feely, R.A., Lorenzoni, L., Molinero, J.-C., Bremer, K., Jones, D.O.B., Iglesias-Rodriguez, D., Greeley, D., Lamare, M.D., Paulmier, A., Graco, M., Cartes, J., e Ramos, J.B., de Lara, A., Sanchez-Leal, R., Jimenez, P., Paparazzo, F.E., Hartman, S.E., Westernströer, U., Küter, M., Benavides, R., da Silva, A.F., Bell, S., Payne, C., Olafsdottir, S., Robinson, K., Jantunen, L.M., Korablev, A., Webster, R.J., Jones, E. M., Gilg, O., du Bois, P.B., Beldowski, J., Ashjian, C., Yahia, N.D., Twining, B., Chen, X.-G., Tseng, L.-C., Hwang, J.-S., Dahms, H.-U., Oschlies, A., 2020. Global variability in seawater Mg:Ca and Sr:Ca ratios in the modern ocean. Proc. Natl. Acad. Sci. 117 (36), 22281–22292. https://doi.org/10.1073/pnas.1918943117.

Leder, J., Swart, P.K., Szmant, A., Dodge, R., 1996. The origin of variations in the isotopic record of scleractinian corals: I. Oxygen. Geochim. Cosmochim. Acta 60 (15), 2857–2870.

Leonard, N.D., Welsh, K.J., Nguyen, A.D., Sadler, J., Pandolfi, J.M., Clark, T.R., Webb, G. E., Zhao, J.x., Feng, Y.x., 2019. High resolution geochemical analysis of massive *Porites* spp. corals from the Wet Tropics, Great Barrier Reef: rare earth elements, yttrium and barium as indicators of terrigenous input. Mar. Pollut. Bull. 149, 110634. https://doi.org/10.1016/j.marpolbul.2019.110634.

Lewis, S.E., Lough, L.M., Cantin, N.E., Matson, E.G., Kinsley, L., Bainbridge, Z.T., Brodie, J.E., 2018. A critical evaluation of coral Ba/Ca, Mn/Ca and Y/Ca ratios as indicators of terrestrial input: new data from the Great Barrier Reef, Australia. Geochim. Cosmochim. Acta 237, 131–154. https://doi.org/10.1016/j.gca.2018.06.017.

Li, Y.-H., Chan, L.-H., 1979. Desorption of Ba and ^{226}Ra from river-borne sediments in the Hudson estuary. Earth Planet. Sci. Lett. 43 (3), 343–350.

Li, Y., Nowlin Jr., W., Reid, R., 1997. Mean hydrographic fields and their interannual variability over the Texas-Louisiana continental shelf in spring, summer, and fall. J. Geophys. Res. Oceans 102 (C1), 1027–1049.

Liu, Y., Li, X., Zeng, Z., Yu, H.-M., Huang, F., Felis, T., Shen, C.-C., 2019. Annually-resolved coral skeletal $\delta^{138/134}$Ba records: A new proxy for oceanic Ba cycling. Geochim. Cosmochim. Acta 247, 27–39. https://doi.org/10.1016/j.gca.2018.12.022.

Livingston, H.D., Thompson, G., 1971. Trace element concentrations in some modern corals. Limnol. Oceanogr. 16 (5), 786–796.

Lo, L., Shen, C.-C., Lu, C.-J., Chen, Y.-C., Chang, C.-C., Wei, K.-Y., Qu, D., Gagan, M.K., 2014. Determination of element/Ca ratios in foraminifera and corals using cold-and hot-plasma techniques in inductively coupled plasma sector field mass spectrometry. J. Asian Earth Sci. 81, 115–122. https://doi.org/10.1016/j.jseaes.2013.11.016.

Lough, J.M., Cooper, T.F., 2011. New insights from coral growth band studies in an era of rapid environmental change. Earth Sci. Rev. 108 (3–4), 170–184. https://doi.org/10.1016/j.earscirev.2011.07.001.

McCulloch, M., Fallon, S., Wyndham, T., Hendy, E., Lough, J., Barnes, D., 2003. Coral record of increased sediment flux to the inner Great Barrier Reef since European settlement. Nature 421 (6924), 727–730. https://doi.org/10.1038/nature01361.

Mitsuguchi, T., Matsumoto, E., Abe, O., Uchida, T., Isdale, P.J., 1996. Mg/Ca thermometry in coral skeletons. Science 274 (5289), 961–963.

Montaggioni, L.F., Le Cornec, F., Corrège, T., Cabioch, G., 2006. Coral barium/calcium record of mid-Holocene upwelling activity in New Caledonia, south-west Pacific. Palaeogeogr. Palaeoclimatol. Palaeoecol. 237 (2–4), 436–455. https://doi.org/10.1016/j.palaeo.2005.12.018.

Moore, W.S., 1997. High fluxes of radium and barium from the mouth of the Ganges-Brahmaputra River during low river discharge suggest a large groundwater source. Earth Planet. Sci. Lett. 150 (1–2), 141–150.

Moyer, R.P., Grottoli, A.G., Olesik, J.W., 2012. A multiproxy record of terrestrial inputs to the coastal ocean using minor and trace elements (Ba/Ca, Mn/Ca, Y/Ca) and carbon isotopes (δ^{13}C, Δ^{14}C) in a nearshore coral from Puerto Rico. Paleoceanography 27 (3), PA3205. https://doi.org/10.1029/2011PA002249.

Moynihan, M.A., Amini, S., Goodkin, N.F., Tanzil, J.T.I., Chua, J.Q.I., Fabbro, G.N., Fan, T.-Y., Schmidt, D.N., Miserez, A., 2021. Environmental impact on the mechanical properties of *Porites* spp. corals. Coral Reefs 40, 701–717. https://doi.org/10.1007/s00338-021-02064-3.

Müller-Karger, F.E., Walsh, J.J., Evans, R.H., Meyers, M.B., 1991. On the seasonal phytoplankton concentration and sea surface temperature cycles of the Gulf of Mexico as determined by satellites. J. Geophys. Res. 96 (C7), 12645–12665. https://doi.org/10.1029/91JC00787.

Murray, S.P., Jarosz, E., Weeks III, E.T., 1998. An observational study of the Mississippi-Atchafalaya coastal plume: Final report. U.S. Department of the Interior, Minerals Management Service, Gulf of Mexico OCS Region, New Orleans, LA.

Nagtegaal, R., Grove, C.A., Kasper, S., Zinke, J., Boer, W., Brummer, G.-J.A., 2012. Spectral luminescence and geochemistry of coral aragonite: Effects of whole-core treatment. Chem. Geol. 318, 6–15. https://doi.org/10.1016/j.chemgeo.2012.05.006.

National Weather Service, 2019. Mississippi River flood history 1543-present. URL https://www.weather.gov/lix/ms_flood_history (accessed 07.14.2020).

Okai, T., Suzuki, A., Kawahata, H., Terashima, S., Imai, N., 2002. Preparation of a new geological survey of Japan geochemical reference material: coral JCp-1. Geostand. Newslett. 26 (1), 95–99.

Ourbak, T., Corrège, T., Malaizé, B., Le Cornec, F., Charlier, K., Peypouquet, J.P., 2006. A high-resolution investigation of temperature, salinity, and upwelling activity proxies in corals. Geochem. Geophys. Geosyst. 7 (3), Q03013. https://doi.org/10.1029/2005GC001064.

Paillard, D., Labeyrie, L., Yiou, P., 1996. Macintosh program performs time-series analysis. EOS, Transactions American Geophysical Union 77 (39), 379. https://doi.org/10.1029/96EO00259.

Pingitore, N.E., Rangel, Y., Kwarteng, A., 1989. Barium variation in *Acropora palmata* and *Montastrea annularis*. Coral Reefs 8, 31–36. https://doi.org/10.1007/bf00304689.

Priest, T., 2007. Extraction not creation: The history of offshore petroleum in the Gulf of Mexico. Enterp. Soc. 8, 227–267. https://doi.org/10.1093/es/khm027.

Prouty, N.G., Field, M.E., Stock, J.D., Jupiter, S.D., McCulloch, M., 2010. Coral Ba/Ca records of sediment input to the fringing reef of the southshore of Moloka'i, Hawai'i over the last several decades. Mar. Pollut. Bull. 60 (10), 1822–1835. https://doi.org/10.1016/j.marpolbul.2010.05.024.

Quinn, T.M., Sampson, D.E., 2002. A multiproxy approach to reconstructing sea surface conditions using coral skeleton geochemistry. Paleoceanography 17 (4), 1062. https://doi.org/10.1029/2000PA000528.

Rabalais, N.R., Turner, R.E., 2001. Hypoxia in the Northern Gulf of Mexico: Description, causes and change. In: Rabalais, N.R., Turner, R.E. (Eds.), Coastal Hypoxia: Consequences for Living Resources and Ecosystem, Vol. 58. American Geophysical Union, Washington D.C., pp. 1–36. https://doi.org/10.1029/CE058p0001

Rabalais, N.N., Turner, E., Dortch, Q., Justic, D., Bierman Jr., V.J., Wiseman Jr., W.J., 2002. Nutrient-enhanced productivity in the northern Gulf of Mexico: past, present and future. In: Orive, E., Elliott, M., de Jonge, V.N. (Eds.), Nutrients and Eutrophication in Estuaries and Coastal Waters. Developments in Hydrobiology, Vol. 164. Springer, Dordrecht, pp. 39–63. https://doi.org/10.1007/978-94-017-2464-7_4.

Rabalais, N.N., Turner, R.E., Wiseman, W.J., Boesch, D.F., 1991. A brief summary of hypoxia on the northern Gulf of Mexico continental shelf: 1985–1988. Geol. Soc. Lond., Spec. Publ. 58 (1), 35–47.

Reich, C.D., Kuffner, I.B., Hickey, T.D., Morrison, J.M., Flannery, J.A., 2013. Complexity of nearshore strontium-to-calcium ratio variability in a core sample of the massive coral *Siderastrea siderea* obtained in Coral Bay, St. John, US Virgin Islands. In: US Department of the Interior, U.S. Geological Survey Open-File Report 2013-1092. USGS, Washington DC. http://pubs.er.usgs.gov/publication/ofr20131092.

Reuer, M.K., Boyle, E.A., Cole, J.E., 2003. A mid-twentieth century reduction in tropical upwelling inferred from coralline trace element proxies. Earth Planet. Sci. Lett. 210 (3–4), 437–452.

Reynolds, R.W., Rayner, N.A., Smith, T.M., Stokes, D.C., Wang, W., 2002. An improved in situ and satellite SST analysis for climate. J. Clim. 15 (13), 1609–1625. https://doi.org/10.1175/1520-0442(2002)015<1609:AIISAS>2.0.CO;2.

Reynolds, R.W., Smith, T.M., 1994. Improved global sea surface temperature analyses using optimum interpolation. J. Clim. 7 (6), 929–948. https://doi.org/10.1175/1520-0442(1994)007<0929:IGSSTA>2.0.CO;2.

Rosenheim, B.E., Swart, P.K., Thorrold, S.R., 2005. Minor and trace elements in sclerosponge *Ceratoporella nicholsoni*: biogenic aragonite near the inorganic endmember? Palaeogeogr. Palaeoclimatol. Palaeoecol. 228 (1–2), 109–129.

Ross, C.L., DeCarlo, T.M., McCulloch, M.T., 2019. Calibration of Sr/Ca, Li/Mg and Sr-U paleothermometry in branching and foliose corals. Paleoceanogr. Paleoclimatol. 34 (8), 1271–1291. https://doi.org/10.1029/2018PA003426.

Sadler, J., Webb, G.E., Nothdurft, L.D., Dechnik, B., 2014. Geochemistry-based coral palaeoclimate studies and the potential of 'non-traditional' (non-massive *Porites*) corals: Recent developments and future progression. Earth Sci. Rev. 139, 291–316. https://doi.org/10.1016/j.earscirev.2014.10.002.

Saenger, C., Cohen, A.L., Oppo, D.W., Halley, R.B., Carilli, J.E., 2009. Surface-temperature trends and variability in the low-latitude North Atlantic since 1552. Nat. Geosci. 2 (7), 492–495. https://doi.org/10.1038/ngeo552.

Saha, N., Rodriguez-Ramirez, A., Nguyen, A.D., Clark, T.R., Zhao, J.-X., Webb, G.E., 2018. Seasonal to decadal scale influence of environmental drivers on Ba/Ca and Y/Ca in coral aragonite from the southern Great Barrier Reef. Sci. Total Environ. 639, 1099–1109. https://doi.org/10.1016/j.scitotenv.2018.05.156.

Saha, N., Webb, G.E., Christy, A.G., Zhao, J.-x., 2019. Vanadium in the massive coral *Porites*: a potential proxy for historical wood clearing and burning. Earth Planet. Sci. Lett. 527, 115793 https://doi.org/10.1016/j.epsl.2019.115793.

Schiller, R.V., Kourafalou, V.H., Hogan, P., Walker, N.D., 2011. The dynamics of the Mississippi River plume: Impact of topography, wind and offshore forcing on the fate of plume waters. J. Geophys. Res. 116 (C6), C06029 https://doi.org/10.1029/2010jc006883.

Schmahl, G.P., Hickerson, E.L., Precht, W.F., 2008. Biology and ecology of coral reefs and coral communities in the Flower Garden Banks region, northwestern Gulf of Mexico. In: Coral Reefs of the USA. Springer, Dordrecht, pp. 221–261.

Schrag, D.P., 1999. Rapid analysis of high precision Sr/Ca ratios in corals and other marine carbonates. Palaeogeography 14 (2), 97–102. https://doi.org/10.1029/1998PA900025.

Shaw, T.J., Moore, W.S., Kloepfer, J., Sochaski, M.A., 1998. The flux of barium to the coastal waters of the southeastern USA: the importance of submarine groundwater discharge. Geochim. Cosmochim. Acta 62 (18), 3047–3054.

Shen, C.-C., Cheng, H., Edwards, R.L., Moran, S.B., Edmonds, H.N., Hoff, J.A., Thomas, R. B., 2003. Measurement of attogram quantities of ^{231}Pa in dissolved and particulate fractions of seawater by isotope dilution thermal ionization mass spectroscopy. Anal. Chem. 75 (5), 1075–1079. https://doi.org/10.1021/ac026247r.

Shen, C.-C., Li, K.-S., Sieh, K., Natawidjaja, D., Cheng, H., Wang, X., Edwards, R.L., Lam, D.D., Hsieh, Y.-T., Fan, T.-Y., Meltzner, A.J., Taylor, F.W., Quinn, T.M., Chiang, H.-W., Kilbourne, K.H., 2008. Variation of initial ^{230}Th/^{232}Th and limits of high precision U-Th dating of shallow-water corals. Geochim. Cosmochim. Acta 72 (17), 4201–4223. https://doi.org/10.1016/j.gca.2008.06.011.

Shen, C.-C., Wu, C.-C., Cheng, H., Edwards, R.L., Hsieh, Y.T., Gallet, S., Chang, C.-C., Li, T.-Y., Lam, D.D., Kano, A., Hori, M., Spötl, C., 2012. High-precision and high-resolution carbonate ^{230}Th dating by MC-ICP-MS with SEM protocols. Geochim. Cosmochim. Acta 99, 71–86. https://doi.org/10.1016/j.gca.2012.09.018.

Shen, G.T., Sanford, C.L., 1990. Trace element indicators of climate variability in reef-building corals. In: Glynn, P.W. (Ed.), Global ecological consequences of the 1982–83 El Nino-Southern Oscillation. Elsevier, pp. 255–283.

Shen, G.T., Cole, J.E., Lea, D.W., Linn, L.J., McConnaughey, T.A., Fairbanks, R.G., 1992. Surface ocean variability at Galapagos from 1936–1982: Calibration of geochemical tracers in corals. Paleoceanography 7 (5), 563–588. https://doi.org/10.1029/92PA01825.

Sinclair, D.J., 2005. Non-river flood barium signals in the skeletons of corals from coastal Queensland, Australia. Earth Planetary Sci. Lett. 237 (3–4), 354–369. https://doi.org/10.1016/j.epsl.2005.06.039.

Sinclair, D.J., McCulloch, M.T., 2004. Corals record low mobile barium concentrations in the Burdekin River during the 1974 flood: evidence for limited Ba supply to rivers? Palaeogeogr. Palaeoclimatol. Palaeoecol. 214 (1–2), 155–174. https://doi.org/10.1016/j.palaeo.2004.07.028.

Smith, J.M., Quinn, T.M., Helmle, K.P., Halley, R.B., 2006. Reproducibility of geochemical and climatic signals in the Atlantic coral *Montastraea faveolata*. Paleoceanography 21 (1), PA1010. https://doi.org/10.1029/2005PA001187.

Smith, S.V., Buddemeier, R.W., Redalje, R.C., Houk, J.E., 1979. Strontium-calcium thermometry in coral skeletons. Science 204, 404–406. https://doi.org/10.1126/science.204.4391.404.

Sowa, K., Watanabe, T., Kan, H., Yamano, H., 2014. Influence of land development on Holocene *Porites* coral calcification at Nagura Bay, Ishigaki island, Japan. PLoS One 9 (2), e88790. https://doi.org/10.1371/journal.pone.0088790.

Swart, P., Elderfield, H., Greaves, M., 2002. A high-resolution calibration of Sr/Ca thermometry using the Caribbean coral *Montastraea annularis*. Geochem. Geophys. Geosyst. 3 (11), 1–11. https://doi.org/10.1029/2002GC000306.

Swart, P.K., Healy, G., Greer, L., Lutz, M., Saied, A., Anderegg, D., Dodge, R.E., Rudnick, D., 1999. The use of proxy chemical records in coral skeletons to ascertain past environmental conditions in Florida Bay. Estuaries 22 (2), 384–397. https://doi.org/10.2307/1353206.

Tanzil, J.T.I., Goodkin, N.F., Sin, T.M., Chen, M.L., Fabbro, G.N., Boyle, E.A., Lee, A.C., Toh, K.B., 2019. Multi-colony coral skeletal Ba/Ca from Singapore's turbid urban reefs: relationship with contemporaneous in-situ seawater parameters. Geochim. Cosmochim. Acta 250, 191–208. https://doi.org/10.1016/j.gca.2019.01.034.

Teague, W.J., Wijesekera, H.W., Jarosz, E., Fribance, D.B., Lugo-Fernández, A., Hallock, Z.R., 2013. Current and hydrographic conditions at the East Flower Garden Bank in 2011. Cont. Shelf Res. 63, 43–58. https://doi.org/10.1016/j.csr.2013.04.039.

Toth, L.T., Aronson, R.B., Kobb, K.M., Cheng, H., Edwards, R.L., Grothe, P.R., Sayani, H. R., 2015. Climatic and biotic thresholds of coral-reef shutdown. Nat. Clim. Chang. 5 (4), 369–374. https://doi.org/10.1038/nclimate2541.

Trefry, J.H., Trocine, R.P., McElvaine, M.L., Rember, R.D., Hawkins, L.T., 2007. Total mercury and methylmercury in sediments near offshore drilling sites in the Gulf of Mexico. Environ. Geol. 53 (2), 375–385. https://doi.org/10.1007/s00254-007-0653-6.

Tudhope, A.W., Lea, D.W., Shimmield, G.B., Chilcott, C.P., Head, S., 1996. Monsoon climate and Arabian Sea coastal upwelling recorded in massive corals from southern Oman. Palaios 11 (4), 347–361.

Tudhope, R., Lea, D.W., Shimmield, G.B., Chilcott, C.P., Scoffin, T.P., Fallick, A.E., Jebb, M., 1997. Climatic records from massive *Porites* corals in Papua New Guinea: A comparison of skeletal Ba/Ca, skeletal $\delta^{18}O$, and coastal rainfall. In: Lessios, H.A., Macintyre, I.G. (Eds.), Proceedings of the 8th Interntional Coral Reef Symposium, 2. Smithsonian Tropical Research Institute, Panama, pp. 1719–1724.

Turner, R.E., Milan, C.S., Rabalais, N.N., 2004. A retrospective analysis of trace metals, C, N and diatom remnants in sediments from the Mississippi River delta shelf. Mar. Pollut. Bull. 49 (7–8), 548–556. https://doi.org/10.1016/j.marpolbul.2004.03.013.

Veron, J.E.N., 1995. Corals in Space and Time. In: The Biogeography and Evolution of the Scleractinia. Comstock/Cornell, Ithaca and London.

Wagner, A.J., Slowey, N.C., 2011. Oxygen isotopes in seawater from the Texas-Louisiana shelf. Bull. Mar. Sci. 87 (1), 1–12. https://doi.org/10.5343/bms.2010.1004.

Walker, N.D., 2005. Wind and eddy-related shelf/slope circulation processes and coastal upwelling in the Northwestern Gulf of Mexico. In: Sturges, W., Lugo-Fernandez, A. (Eds.), Circulation in the Gulf of Mexico: Observations and Models, Vol. 161. American Geophyscial Union, Washington DC, pp. 295–313. https://doi.org/10.1029/161GM21.

Walker, N.D., Leben, R.R., Balasubramanian, S., 2005. Hurricane-forced upwelling and chlorophyll-a enhancement within cold-core cyclones in the Gulf of Mexico. Geophys. Res. Lett. 32 (18), L18610 https://doi.org/10.1029/2005gl023716.

Walther, B.D., Kingsford, M.J., McCulloch, M.T., 2013. Environmental records from Great Barrier Reef corals: inshore versus offshore drivers. PLoS One 8 (10), e77091. https://doi.org/10.1371/journal.pone.0077091.

Weber, J.N., 1973. Incorporation of strontium into reef coral skeletal carbonate. Geochim. Cosmochim. Acta 37 (9), 2173–2190. https://doi.org/10.1016/0016-7037(73)90015-x.

Weber, J.N., 1974. Skeletal chemistry of scleractinian reef corals: Uptake of magnesium from seawater. Am. J. Sci. 274 (1), 84–93.

Wei, G., McCulloch, M.T., Mortimer, G., Deng, W., Xie, L., 2009. Evidence for ocean acidification in the Great Barrier Reef of Australia. Geochim. Cosmochim. Acta 73 (8), 2332–2346. https://doi.org/10.1016/j.gca.2009.02.009.

Wiseman, W.J., Rabalais, N., Turner, R., Dinnel, S., MacNaughton, A., 1997. Seasonal and interannual variability within the Louisiana coastal current: stratification and hypoxia. J. Mar. Syst. 12 (1–4), 237–248.

Wyndham, T., McCulloch, M., Fallon, S., Alibert, C., 2004. High-resolution coral records of rare earth elements in coastal seawater: biogeochemical cycling and a new environmental proxy. Geochim. Cosmochim. Acta 68 (9), 2067–2080. https://doi.org/10.1016/j.gca.2003.11.004.

Yamazaki, A., Watanabe, T., Ogawa, N.O., Ohkouchi, N., Shirai, K., Toratani, M., Uematsu, M., 2011. Seasonal variations in the nitrogen isotope composition of Okinotori coral in the tropical western Pacific: a new proxy for marine nitrate dynamics. J. Geophys. Res. Biogeosci. 116 (G4), G04005 https://doi.org/10.1029/2011JG001697.

York, D., Evensen, N.M., 2004. Unified equations for the slope, intercept, and standard errors of the best straight line. Am. J. Phys. 72 (3), 367–375. https://doi.org/10.1119/1.1632486.

Yu, T.L., Wang, B.-S., You, C.-F., Burr, G.-S., Chung, C.-H., Chen, Y.-G., 2015. Geochemical effects of biomass burning and land degradation on Lanyu Islet, Taiwan. Limnol. Oceanogr. 60 (2), 411–418. https://doi.org/10.1002/lno.10039.

Supplementary Material for

Insights from barium variability in a *Siderastrea siderea* coral in the northwestern Gulf of Mexico

Mudith M. Weerabaddana [a, b*], Kristine L. DeLong [a, c*], Amy J. Wagner [d], Deborah W.Y. Loke [a], K. Halimeda Kilbourne [e], Niall Slowey [f], Hsun-Ming Hu [g], and Chuan-Chou Shen

Published in Marine Pollution Bulletin, 2021, doi:10.1016/j.marpolbul.2021.112930

Supplementary Table 1

Summary of accuracy and precision for Sr/Ca and Mg/Ca determinations.

LSU	Sr 421 nm/Ca 422 nm			Mg 279 nm/Ca 315 nm		
Reference [a]	IGS	PL	JCp-1	IGS	PL	JCp-1
RSD (%) [b]	0.14	0.274	0.18	1.12	1.58	1.14
Precision (mmol/mol, 1σ)	±0.012	±0.025	±0.007	±0.038	±0.071	±0.082
Accuracy (%) [c]	–0.005	0.092	–0.150	0.015	0.859	3.518
Number of observations	115	201	13	115	201	13
UMCES-CBL						
RSD (%) [b]	0.04%	0.17%	0.18%	0.83%	1.35%	-
Precision (mmol/mol, 1σ)	±0.003	±0.015	±0.016	±0.026	±0.069	-
Accuracy (%) [c]	0.00	–0.13	+0.294	0.02	–1.81	-
Number of observations	80	116	25	80	116	-

[a] IGS is an internal gravimetric standard whereas JCp-1 and PL are external coral references.

[b] Residual standard deviation (%) = (standard deviation (1σ)/average) x100.

[c] Accuracy (%) = ((average–known value)/known value) x100.

Supplementary Table 2

Summary of accuracy and precision for Ba/Ca wavelength combinations.

Reference [a]	IGS	PL	JCp-1	IGS	PL	JCp-1	IGS	PL	JCp-1
	Ba 455 nm/Ca 317 nm			Ba 455 nm/Ca 315 nm			Ba 455 nm/Ca 422 nm		
RSD (%) [b]	1.51	4.67	6.91	1.54	4.65	6.80	1.69	4.61	6.54
Precision [c]	±0.12	±0.16	±0.15	±0.12	±0.16	±0.15	±0.14	±0.16	±0.14
Accuracy (%) [d]	–0.03	2.26	–1.25	0.03	2.14	–1.65	–0.01	2.01	–2.01
Number [e]	115	201	13	115	201	13	115	201	13
	Ba 493 nm/Ca 317 nm			Ba 493 nm/Ca 315 nm			Ba 493 nm/Ca 422 nm		
RSD (%) [b]	2.07	5.53	7.40	2.09	5.52	7.34	2.09	5.58	6.80
Precision [c]	±0.17	±0.19	±0.16	±0.17	±0.19	±0.16	±0.17	±0.19	±0.15
Accuracy (%) [d]	–0.06	2.00	–0.19	–0.06	1.87	–0.58	–0.04	1.75	–0.96
Number [e]	115	201	13	115	201	13	115	201	13

[a] IGS is an internal gravimetric standard whereas JCp-1 and PL are external coral references.

[b] Residual standard deviation (%) = (standard deviation (1σ)/average) x100.

[c] Precision in μmol/mol (1σ).

[d] Accuracy (%) = ((average–known value)/known value) x100.

[e] Number of observations.

Supplementary Table 3

Uranium and thorium isotopic compositions and ^{230}Th ages for corals determined by MC-ICP-MS.

Sample ID	Weight g	^{238}U ppb[a]		^{232}Th ppt		$\delta^{234}U$ measured [a]		$[^{230}Th/^{238}U]$ activity [c]		$[^{230}Th/^{232}Th]$ ppm [d]		Age uncorrected		Age corrected [c,e]		$\delta^{234}U_{initial}$ corrected [b]		Year
WFGB 3-2 top	0.33396	2511.4	±2.2	430.6	±1.6	146.0	±1.7	0.001026	±0.000014	98.6	±1.4	97.7	±1.3	93.7	±2.4	146.0	±1.7	1921.54

Analytical errors are ±2σ of the mean.

[a] $[^{238}U] = [^{235}U] \times 137.77$ (±0.11‰) (Hiess et al., 2012); $\delta^{234}U = ([^{234}U/^{238}U]_{activity} - 1) \times 1000$.

[b] $\delta^{234}U_{initial}$ corrected was calculated based on ^{230}Th age (T), i.e., $\delta^{234}U_{initial} = \delta^{234}U_{measured} \times e^{\lambda 234 * T}$, and T is corrected age.

[c] $[^{230}Th/^{238}U]_{activity} = 1 - e^{-\lambda 230 T} + (\delta^{234}U_{measured}/1000)[\lambda_{230}/(\lambda_{230} - \lambda_{234})](1 - e^{-(\lambda 230 - \lambda 234)T})$, where T is the age.

Decay constants are 9.1705×10^{-6} year^{-1} for ^{230}Th, 2.8221×10^{-6} year^{-1} for ^{234}U (Cheng et al., 2013), and 1.55125×10^{-10} year^{-1} for ^{238}U (Jaffey et al., 1971).

[d] The degree of detrital ^{230}Th contamination is indicated by the $[^{230}Th/^{232}Th]$ atomic ratio instead of the activity ratio.

[e] Age corrections, relative to chemistry date on 11 March 2015, were calculated using an estimated atomic $^{230}Th/^{232}Th$ ratio of 4 ± 2 ppm (Shen et al., 2008).

Supplementary Table 4

Correlation between annual linear extension rate and coral Sr/Ca and coral Ba/Ca.

	05WFGB3-1-A		05WFGB3-1-A1 (1977–2003)		05WFGB3-1-A2 (1932–1943)	
	Sr/Ca	Ba/Ca	Sr/Ca	Ba/Ca	Sr/Ca	Ba/Ca
Pearson's *r*	0.09	0.10	0.11	0.23	–0.30	0.59
p-value	0.61	0.55	0.57	0.3	0.35	0.05
Number [a]	39	39	27	27	12	12

Annual linear extension for suboptimal paths were not considered, only the master time series.

[a] Number of paired observations used to determine correlation and significance.

Supplementary Table 5

Correlation between US Barite and coral Ba/Ca.

1977–2003	Minimum coral Ba/Ca	Average coral Ba/Ca	Maximum coral Ba/Ca
Barite production	*0.48 2-year lag* *0.52 3-year lag*	*0.44 2-year lag* *0.47 3-year lag*	0.32 2-year lag 0.36 3-year lag
Barite consumption	0.34 2-year lag 0.37 3-year lag	0.35 2-year lag 0.30 3-year lag	0.24 2-year lag 0.20 3-year lag

Items in italics are significant at the 5% level, $n = 25$ for a 2-year lag, and $n = 24$ for a 3-year lag.

References

Cheng, H., Edwards, R.L., Shen, C.-C., Polyak, V.J., Asmerom, Y., Woodhead, J., Hellstrom, J., Wang, Y., Kong, X., Spötl, C., 2013. Improvements in ^{230}Th dating, ^{230}Th and ^{234}U half-life values, and U–Th isotopic measurements by multi-collector inductively coupled plasma mass spectrometry. Earth and Planetary Science Letters, 371: 82-91, doi:10.1016/j.epsl.2013.04.006

Jaffey, A., Flynn, K., Glendenin, L., Bentley, W.t., Essling, A., 1971. Precision measurement of half-lives and specific activities of ^{235}U and ^{238}U. Physical review C, 4(5): 1889, doi:10.1103/PhysRevC.4.1889.

Hiess, J., Condon, D.J., McLean, N., Noble, S.R., 2012. ^{238}U/^{235}U systematics in terrestrial uranium-bearing minerals. Science, 335(6076): 1610-1614, doi:10.1126/science.1215507.

Shen, C.-C., Li, K.-S., Sieh, K., Natawidjaja, D., Cheng, H., Wang, X., Edwards, R.L., Lam, D.D., Hsieh, Y.-T., Fan, T.-Y., 2008. Variation of initial ^{230}Th/^{232}Th and limits of high precision U–Th dating of shallow-water corals. Geochimica et Cosmochimica Acta, 72(17): 4201-4223, doi:10.1016/j.gca.2008.06.011.